Wear 448–449 (2020) 203219

Contents lists available at ScienceDirect

Wear

journal homepage: http://www.elsevier.com/locate/wear

# Analytical, numerical and experimental studies on ploughing behaviour in soft metallic coatings

Tanmaya Mishra [a,*], Matthijn de Rooij [a], Meghshyam Shisode [b], Javad Hazrati [b], Dirk J. Schipper [a]

[a] Surface Technology and Tribology, Faculty of Engineering Technology, University of Twente, 7500 AE, Enschede, the Netherlands
[b] Nonlinear Solid Mechanics, Faculty of Engineering Technology, University of Twente, 7500 AE, Enschede, the Netherlands

ARTICLE INFO

*Keywords:*
Friction model
Galvanized steel
Ploughing
Coating
Material point method

ABSTRACT

A coating layer is often present on engineering surfaces. An example is a zinc coating on steel sheet, this being a soft metallic coating on a hard substrate. To characterize the tribological behaviour of these engineered surfaces, it is necessary to understand the mechanical behaviour of the coating during ploughing. The material point method (MPM)-based ploughing model has been used to compute friction and the ploughed profile when an asperity is ploughing through a coated surface. An analytical ploughing model has also been used to study the effect of the thickness and hardness of the coating relative to the substrate on coefficient of friction using rigid-plastic material behaviour and its results have been compared with the MPM-model results. The MPM-based ploughing model has been experimentally validated and is shown to agree well with the ploughing experiments using rigid spherical indenters sliding through lubricated-zinc coated steel, uncoated steel and bulk zinc over a range of applied loads.

## 1. Introduction

Zinc coatings are often applied on steel sheets in a molten zinc bath using continuous hot-dip galvanizing to improve their corrosion resistance and paintability. The presence of a zinc coating also affects the friction and wear behaviour of the galvanized sheets which are further used in deep-drawing, stamping and other forming processes [1–3]. Both the thickness and the hardness of the zinc coating are critical for the tribological performance of the galvanized products [1]. In the production process, the thickness of the zinc coating is controlled by using air knives to remove the excess of zinc from the sheets drawn out from the zinc bath [4], while the hardness of the galvanized sheets is varied by alloying the zinc bath with various elements or by annealing the galvanized sheets [5].

During the loading and sliding of the forming tools and galvanized sheets against each other, the harder tool surface flattens the asperities of the softer sheet surface, while the hard tool asperities plough through the flattened sheet surface [6]. The friction force is therefore due to the plastic deformation of the substrate as well as the shearing of the interface [7]. The thickness of the coating and the hardness of the coating relative to the substrate determines the friction and wear mechanisms in a coated system [8]. Furthermore, soft metallic coatings have large scale localised plastic deformation resulting in coating fracture and abrasive wear, these phenomena studied using scratch testing at [9,10]. Hence, numerical ploughing models are critical in computing and understanding friction and wear.

The effect of the properties of the substrate and the coating on the plastic deformation in coated systems have been studied by modelling both indentation and scratching using finite element (FE) models [8,11]. The effect of the ratio of the yield strength of the coating relative to the substrate, on the plastic deformation in the coating has been studied by indenting at different penetration depths [11]. The critical depth, defined as the penetration depth below which the substrate had negligible effect on the deformation in the coating, was shown to decrease with the increase in coating-substrate yield strength ratio and size of the indenter tip [11]. For a coating-substrate yield strength ratio less than 0.1-0.2, the measured critical depth was 0.3 times the coating thickness [11,12]. Harder substrates promote initiation and propagation of plastic deformation in the coating with increased pile-up of the coating material around the indenter [11]. The critical penetration depth was given as a function of the ratios of yield strength and stiffness of the coating and the

* Corresponding author.
*E-mail addresses:* t.mishra@utwente.nl (T. Mishra), m.b.derooij@utwente.nl (M. de Rooij), m.p.shisode@utwente.nl (M. Shisode), j.hazratimarangalou@utwente.nl (J. Hazrati), d.j.schipper@utwente.nl (D.J. Schipper).

https://doi.org/10.1016/j.wear.2020.203219
Received 18 October 2019; Received in revised form 14 January 2020; Accepted 3 February 2020
Available online 10 February 2020

**Nomenclature of symbols**

| | |
|---|---|
| $A_{xy}$ | Projected contact area in the $xy$ plane |
| $A_{yz}$ | Projected contact area in the $yz$ plane |
| $C_0$ | Proportionality constant for interfacial shear |
| $C_p$ | Proportionality constant for contact pressure |
| $E$ | Young modulus |
| $F_n$ | Normal load/force on the indenter |
| $H_{cs}$ | Effective hardness of the coated substrate |
| $H_c$ | Hardness of the coating |
| $H_s$ | Hardness of the substrate |
| $\tilde{H}$ | Relative hardness of coating, $H_c/H_s$ |
| $I$ | Identity matrix |
| $K$ | Bulk Modulus |
| $P_{pl}$ | Contact pressure due to plastic deformation |
| $\overline{P}$ | Mean nominal contact pressure |
| $R_a$ | Mean surface roughness |
| $R_q$ | Root mean squared surface roughness |
| $T_0$ | Contact/ambient temperature |
| $V$ | Volume of particle |
| $\rho$ | Density of the material |
| $\kappa$ | Shear strength of the substrate (bulk) |
| $\kappa_t$ | Thermal conductivity |
| $\tau_{sh}$ | Shear strength of the interface |
| $\tau_{bl}$ | Shear strength of the boundary layer |
| $\sigma_y$ | Yield/flow stress |
| $\sigma_h$ | Hydrostatic stress |
| $\mu$ | Coefficient of friction |
| $a$ | Total contact radius |
| $c$ | Related to the coating (subscript) |
| $d_p$ | Total ploughing depth |
| $d_g$ | Groove depth |
| $d$ | Penetration depth |
| $f$ | Ratio of interfacial to bulk shear strength |
| $h_{pu}$ | Pile up height |
| $k_1$ | Fitting factor for effective hardness |
| $k_0$ | Ratio of interfacial strength to hardness |
| $m$ | Mass of particle |
| $n_P$ | Exponent of pressure |
| $n_v$ | Exponent of sliding velocity |
| $n_T$ | Exponent of temperature |
| $q$ | Heat generated |
| $r$ | Radius of the indenter/asperity |
| $s$ | Related to substrate (subscript) |
| $t$ | Thickness of the coating |
| $t_c$ | Coating thickness for transition in ploughing |
| $v_i$ | Sliding velocity of the indenter |
| $x$ | Related to $x$ axis (sub/superscript) |
| $y$ | Related to $y$ axis (sub/superscript) |
| $z$ | Related to $z$ axis (sub/superscript) |
| $cs$ | Related to coated-substrate (subscript) |
| $pl$ | Related to plastic deformation (subscript) |
| $sh$ | Related to interfacial shear (subscript) |
| M | Volumetric change |

substrate in Ref. [13]. Experimental studies on the effect of coating thickness in single and multi-layer metallic coatings have been done in combination with FE-based indentation models in Refs. [14–16]. The contribution of coating and substrate to ploughing and shear components of friction were also studied experimentally in Ref. [17] while considering elastic recovery in hard coatings on steel. Experimentally validated theories have shown the effect of coating thickness, surface roughness and material properties of the coating and the substrate on friction and wear due to shearing in soft thin coating in Refs. [18–21].

Although FE models for different coated systems have provided a good overview of the deformation response of coatings to indentation, numerical ploughing models are required to understand the dynamic deformation response of coating subjected to ploughing by an asperity. Typically scratch models and experiments are used to study the coating-substrate adhesion and coating damage mechanisms [9]. The scratch behaviour in both hard and soft polymeric coatings has been studied using FE models [22], where the principal stresses along the wear track have been analysed to explain the failure and damage in the coatings. The effects of coating thickness and hardness on deformation and damage have been studied by FE models for scratching in multilayer polymeric coatings [23]. The stresses, strains, damage and friction has been modelled for spherical indenters sliding through hard coated surface using FE models in Ref. [24]. Similarly, critical loads, friction, deformation and damage in coatings and coating-substrate adhesion are also studied for both hard and soft coatings using FE models in Refs. [25,26]. Typically, a linear-elastic material model is used for hard coatings while elastic-plastic material model is used for soft coatings in these FE models. The FE models use adaptive re-meshing techniques to avoid element distortion in modelling large scale plastic deformation which makes these models inefficient. Moreover, constant (Coulomb's law) coefficient of friction is used in the simulation for the shearing of the indenter-coating interface [25,26].

Recently, particle-based, molecular dynamics (MD) models have been used to study nano-indentation and nano-scratch behaviour of multi-layered films [27,28]. The effect of indentation size and coating thickness on the indentation hardness [29] and the effect of indentation depth on adhesion and plastic deformation during loading and unloading has been observed and explained using the slip systems and plastic energy in MD simulations of indentation [27]. MD simulation of scratching processes have been used to explain coating-asperity adhesion, coating-substrate adhesion, plastic deformation, work-hardening, pile-up, stick-slip and wear phenomenon in multi-layer films [28,30] at an atomistic scale. However, the correct choice of interatomic potentials, scaling up and physical validation of results are challenging in MD models.

In modelling of coated systems, it is critical to accurately characterize the material and contact behaviour of the coating. Typically, the hardness and the Young's modulus of a thin coating is measured by nano-indentation considering the properties of the coating with respect to the substrate in Refs. [31–33]. Initial work to measure the effective hardness for single layered coatings was done by Ref. [34] for soft coatings and by Ref. [32] for hard coatings. The effect of indentation size and coating thickness was accounted for in estimating the intrinsic hardness of both hard and soft coated systems using theoretical and FE models and experiments in Ref. [35]. Furthermore, the Young's modulus of thin films can be characterized by the approach given in Refs. [36,37]. Also, the shear strength of the asperity-coating interface needs to be characterized accurately to model friction during ploughing. In the presence of a boundary layer on the coated surface, *e.g.* aluminium and gold coating on glass [38,39], the interfacial shear strength is characterized as a function of applied load [40].

The elastic and plastic properties of zinc coating on steel sheets have been characterized by tensile tests in Refs. [41,42] and by nano-indentation in Refs. [43–46]. However, there is still lack of sufficient data on the material, contact and interfacial properties of galvanized steel sheets. Moreover, the numerical models available for coated systems have mostly studied either indentation or scratching behaviour for hard-metallic or polymeric coatings relevant to their damage and

failure mechanisms. The available FE and MD based numerical scratch/ploughing models for coated systems lack accurate experimental validation of the ploughing friction. Also, specific numerical ploughing models for zinc coatings, in the galvanized steel sheets, are absent in the literature to the knowledge of the authors.

Recently, the material point method (MPM) has been successfully used to model ploughing in steel for various loads and indenter sizes [47]. The MPM-based ploughing model combines features of both particle and mesh based numerical methods to measure friction and wear in lubricated steel sheets with experimental validation. Also the interfacial shear strength of lubricated zinc coating has been measured for a range of loads in Ref. [48]. The current research has focussed on extending the MPM-based ploughing model for lubricated, zinc coated steel sheets. A theoretical study on the effect of the coating thickness and hardness of the coating relative to the substrate on ploughing friction and ploughing depth has been done and compared with the MPM-based ploughing model for coated-systems with a rigid-plastic (negligible elastic recovery and work hardening) material behaviour. The size of the indenter, thickness of the zinc coating and applied load have been varied to study their effect on ploughing friction and wear. The MPM model results for zinc coated steel sheets are experimentally validated and compared with ploughing experiments of uncoated steel sheets and zinc blocks. The results have been explained using the available literature on characterization of soft, thin coatings.

## 2. Calculation of friction in ploughing of coated systems

Before the MPM simulations of ploughing is discussed, an approximate analytical model has been developed to investigate the expected effect of parameters such as coating thickness and hardness on the frictional behaviour in ploughing of the coatings. The analytical model is based on the concept of load sharing in a coated system in contact with a rigid-counter face, given in Refs. [20,49], and [21]. Rigid-plastic material behaviour is chosen for the coated system. The analytical model will consist of a contact model to compute the contact area between the asperity sliding through the coated substrate. Using the calculated contact area and the hardness of coating, substrate and coated system the ploughing friction will be calculated. As mentioned, the analytical model will be used to understand the factors contributing to ploughing friction and to compare and explain the results obtained from the numerical (MPM) ploughing model and ploughing experiments on coated systems respectively.

A rigid spherical indenter sliding through a rigid-plastic coated system could result in two contacting conditions. In the first case, the spherical indenter is only in contact with the coating, *i.e.* the ploughing depth $d_p$ is less than the coating thickness $t$. In the second case, the spherical indenter is in contact with both the coating and the substrate, *i.e.* the ploughing depth is more than the coating thickness.

The response to loading (indentation) of a coated system is determined from its effective hardness $H_{cs}$. The effective hardness of a coated system $H_{cs}$ is given by combining the hardness of the substrate ($H_s$) and the hardness of the coating ($H_c$) typically by using a rule of mixtures. The hardness $H_{cs}$ is obtained as a function of coating thickness $t$ from the indentation response to a spherical indenter. For thin, soft coatings on hard substrates the effective hardness is given using equation (1) [50]. The value $k_1 = 125$ was obtained by experimentally fitting the indentation response of spheres of various radii ($r$) on a coated substrate, where $H_{cs} \approx H_c$ for values of $t/r \geq 0.04$ [50].

$$H_{cs} = H_c + (H_s - H_c)\exp\left(-k_1\frac{t}{r}\right) \tag{1}$$

### 2.1. Calculation of contact area in ploughing of a coated substrate

For a spherical indenter of radius $r$, ploughing through the coated substrate with ploughing depth less than or equal to the coating thickness ($d_p \leq t$), the contact radius is taken as $a$. Considering the frontal half of the indenter in contact during ploughing through the coating in a rigid-plastic coated-substrate (see Fig. 1a), the horizontal projection $A_{xy}$ of the total contact area is determined. By dividing the applied load $F_n$ by the mean contact pressure $P_{pl}$ (due to plastic deformation), the horizontal projection (in the '$xy$ plane') of the contact area $A_{xy}$ is obtained, see equation (2.1). For normal loading of a plastically deforming coated substrate, the contact pressure $P_{pl}$ equals the effective indentation hardness $H_{cs}$ of the coated system. The ploughing depth $d_p$ for a spherical indenter of radius $r$ is obtained from its contact radius as given in equation (2.2). The (vertical) cross-sectional contact area $A_{yz}$ for a spherical indenter ploughing in $x$ direction is given as the area of the segment formed by the intersection of the contact plane on the indenter's 'mid $yz$-plane' and is expressed in equation (2.3) [47] (see Fig. 1b).

$$A_{xy} = \frac{\pi a^2}{2} = \frac{F_n}{H_{cs}} \tag{2.1}$$

$$d_p = r - \sqrt{r^2 - a^2} \tag{2.2}$$

$$A_{yz} = r^2 \operatorname{atan}\frac{a}{r - d_p} - a(r - d_p) \tag{2.3}$$

Fig. 1 shows the case of a rigid spherical indenter ploughing through both the coating and the substrate. So, $d_p > t$. The total ploughing depth $d_p$ is given as the sum of ploughing depth in the substrate $d_s$ and ploughing depth in the coating $d_c$. In this case $d_c = t$, as $d_p > t$. The applied normal load $F_n$ is now carried by both the coating and the substrate over the total contact area $A_{xy} = A_{xy_s} + A_{xy_c}$ where $A_{xy_s}$ is the contact area of the substrate and $A_{xy_c}$ is the contact area of the coating, (see Fig. 1c). It is assumed that the contact pressure generated in the coating equals the effective hardness of the coated system $H_{cs}$, while the contact pressure in the substrate equals hardness of the substrate $H_s$. The contact area of the coating with the indenter $A_{xy_c}$ (the area of the annular semi-circle in Fig. 1c) is given in equation (3.1) in terms of the ploughing depth in the substrate $d_s$, indenter radius $r$ and coating thickness $t$ (using equation (2.2) for $d_p = d_s + t$). By equating the applied load to the contact pressure in the contact area with the coating and the substrate and substituting expression of $A_{xy_c}$ from equation (3.1), the expression of $d_s$ can be calculated by solving the resulting quadratic equation in equation (3.2), and choosing the one feasible solution of $d_s$ (the $d_s < r$).The horizontal and vertical projections of the contact area with the substrate $A_{xy_c}$ and $A_{yz_s}$, are given in equations (3.3) and (3.4) respectively. The total horizontal projection $A_{yz}$ of the indenter with the coated substrate is now given by substituting $d_p = d_s + t$ in equation (2.3). The vertical projection of the contact area of the indenter with the coating $A_{yz_c}$ is given as the difference between $A_{yz}$ and $A_{yz_s}$ in equation (3.5) (see Fig. 1b).

$$\begin{aligned} &A_{xy_c} = A_{xy} - A_{xy_s} = 0.5\pi\left(a^2 - a_s^2\right) = 0.5\pi\left(r^2 - \left(r - d_p\right)^2 - \left(r^2 - \left(r - d_s\right)^2\right)\right) \\ &\Rightarrow A_{xy_c} = 0.5\pi t(2(r - d_s) - t) \end{aligned} \tag{3.1}$$

$$\begin{aligned} &H_s A_{xy_s} + H_{cs} A_{xy_c} = F_n \Rightarrow 0.5\pi\left(r^2 - \left(r - d_s\right)^2\right)H_s = F_n - 0.5\pi t(2(r - d_s) - t)H_{cs} \\ &\Rightarrow 0.5\pi H_s d_s^2 + \pi(H_{cs}t - H_s r)d_s + F_n - 0.5\pi t(2r - t)H_{cs} = 0 \\ &\Rightarrow d_s = -\frac{B + \sqrt{B^2 - 4AC}}{2A} \forall A = 0.5\pi H_s,\ B = \pi(H_{cs}t - H_s r), \\ &C = F_n - 0.5\pi t(2r - t)H_{cs} \end{aligned} \tag{3.2}$$

$$A_{xy_s} = 0.5\pi\left(r^2 - \left(r - d_s\right)^2\right) \tag{3.3}$$

$$A_{yz_s} = r^2 \operatorname{atan}\left(\frac{a_s}{r - d_s}\right) - a_s(r - d_s) \ \forall a_s = \sqrt{r^2 - \left(r - d_s\right)^2} \tag{3.4}$$

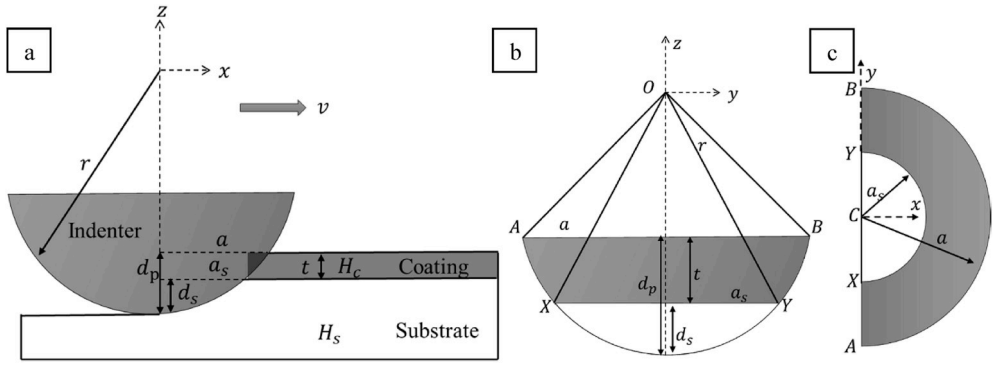


**Fig. 1.** (a) Schematic of a spherical indenter of radius $r$ ploughing through a rigid-plastic coated substrate, with coating thickness $t$, coating hardness $H_c$, substrate hardness $H_s$. (b) The frontal projection of the contact area of the indenter showing total ploughing depth $d_p$, ploughing depth into the substrate $d_s$. (c) The horizontal projection of the contact area showing total contact radius $a$ and contact radius with the substrate $a_s$. (Coating in grey and substrate in white).

$$A_{yz_c} = A_{yz} - A_{yz_s} \; \forall A_{yz} = r^2 \operatorname{atan}\left(\frac{a}{r - d_s - t}\right) - a(r - d_s - t) \text{ and } a = \sqrt{r^2 - (r - d_s - t)^2} \tag{3.5}$$

An algorithm to compute the projection of contact area of the indenter sliding through a coated substrate is shown in Fig. 2. The algorithm accounts for both the cases of contact between the indenter and the coated substrate, *i.e.* indenter with the coating and the indenter with both the coating and the substrate. An initial prediction of the ploughing depth of the spherical indenter is made by equating the applied load with the effective indentation hardness $H_{cs}$. The ploughing depth is compared with the coating thickness to categorize the contact condition amongst the two cases described above. Following the set of equations 2.1-2.3 and 3.1- 3.5 the algorithm computes the contact areas for each of the cases.

### 2.2. Calculation of components of ploughing friction force

The ploughing friction is calculated as the sum of the friction force due to plastic deformation of the ploughed specimen and the friction force due to shearing of the interface [7]. The friction force $F_f$ acting on a spherical asperity ploughing through a specimen is given in equation (4.1). The friction force due to ploughing is given as the product of the contact pressure due to the plastic deformation of the substrate $P_{pl}$ and the area of the ploughed cross section $A_{yz}$. The friction force due to shearing of the interface is given as the product of the interfacial shear strength $\tau_{sh}$ and the contact area between the indenter and the specimen at the surface $A_{xy}$. The overall coefficient of friction $\mu$ is calculated using equation (4.2).

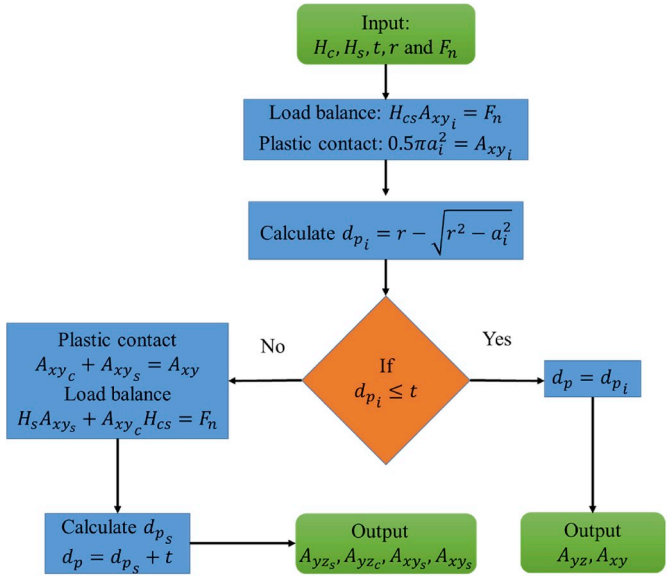


**Fig. 2.** Algorithm to calculate the projected contact areas in the horizontal $xy$ plane $A_{sh}$ and vertical $xz$ plane $A_{pl}$ for a rigid-sphere ploughing through a rigid plastic coated system in $x$ direction.

$$F_f = F_{pl} + F_{sh} = P_{pl}A_{yz} + \tau_{sh}A_{xy} \tag{4.1}$$

$$\mu = \frac{F_f}{F_n} = \mu_{pl} + \mu_{sh} = \frac{P_{pl}A_{yz} + \tau_{sh}A_{xy}}{F_n} \tag{4.2}$$

$$\mu_{pl} = \frac{F_{pl}}{F_n} = \frac{H_s A_{yz_s} + H_c A_{yz_c}}{F_n} \tag{4.3}$$

$$\mu_{sh} = \frac{F_{sh}}{F_n} = \frac{f_s H_s A_{xy_s} + f_c H_c A_{xy_c}}{3\sqrt{3}F_n} \tag{4.4}$$

In ploughing through a rigid-plastic coated substrate, the stress acting on the ploughed cross section $p_{pl}$ are taken as the hardness of the coating $H_c$ or hardness of the substrate $H_s$. The coefficient of friction due to plastic deformation of the coated system $\mu_{pl}$ is obtained using equation (4.3), where the friction force due to ploughing is shared by the vertical projected areas of the coating $A_{yz_c}$ and the substrate $A_{yz_s}$. The shear stresses at the indenter-coating contact and the indenter-substrate contact are taken as fractions ($f$), $f_c$ and $f_s$ of the maximum shear strength of the coating $\tau_{shc}$ and the substrate $\tau_{shs}$ respectively. Typically for very clean surfaces, $f = 1$. For a rigid-plastic material, its shear strength $\tau_{sh}$ is given as a factor $1/k_0$ of its hardness $H$. Typically for metals $k_0 = 3\sqrt{3}$ [10,51]. The interfacial friction due to shearing of the substrate and the coating is given by $f_s\tau_{sh_s}$ and $f_c\tau_{sh_c}$ respectively distributed over the horizontal projected areas $A_{xy_s}$ and $A_{xy_c}$ respectively. The coefficient of friction due to shearing of the interface $\mu_{sh}$ in a coated system is given in equation (4.4). If $d_p < t$, the coefficient of friction is given by substituting $A_{yz_s} = 0$ and $A_{xy_s} = 0$ in equations (4.3) and (4.4) respectively. The variations in $\mu_{pl}$, $\mu_{sh}$ and $\mu$ with coating thickness $t$for a soft and a hard coating and with relative coating hardness (hardness ratio) $\tilde{H} = H_c/H_s$ are illustrated in Fig. 3a, 3b and 3c respectively.

The shearing of the contact interface (on the vertical plane in the yz plane) also results in a component for force $F_{sh}^z$ along the loading $z$ direction. Hence the shear stress is carried by vertical contact areas of the substrate $A_{yz_s}$ and the coating $A_{yz_c}$. In ploughing using an applied load of $F_n$ in $-z$ direction, $F_{sh}^z$ acts on the indenter in the $z$ direction. The ratio of $F_{sh}^z$ and $F_n$ is given for a coated system as a factor of $\mu_{pl}^z$ in equation (5.1). The total normal load $F_n^{'}$ acting on the indenter in $z$ direction is now corrected by adding the force due to shear stress $F_{sh}^z$ to applied load $F_n$. The contact area deformation and hence the ploughing depth of the

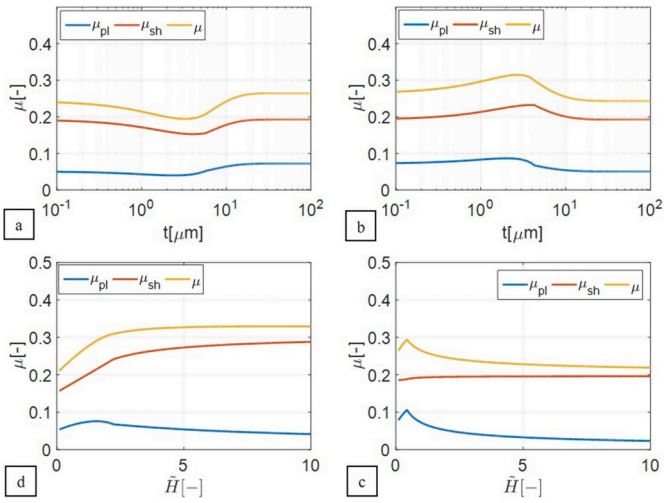


**Fig. 3.** Coefficient of friction due to ploughing of rigid-plastic coated substrate by 1 mm diameter indenter at $F_n = 5$N as a function of (a) coating thickness for a soft coating ($\tilde{H} = 0.5$, $H_s = 900$ MPa) and (b) hard coating ($\tilde{H} = 2$, $H_s = 450$ MPa) ($k_1 = 12.5$). (c) Effect of relative coating hardness $\tilde{H}$ ($H_s = 450$MPa) on ploughing coefficient of friction for coating thickness $t = 4$ μm and (d) $t = 16$ μm.

coated system is corrected using the load $F_n$ in equation (2.1)–(2.3) and equation (3.1)–(3.5) [52]. Also the friction forces are computed with the new contact areas in equation (4.1)–(4.4).

$$\mu_{sh}^{z} = \frac{F_{sh}^{z}}{F_n} = \frac{\tau_s A_{yz_s} + \tau_c A_{yz_c}}{F_n} = \frac{1}{k_0}\mu_{pl} \tag{5.1}$$

$$F_n^{'} = F_n - F_{sh}^{z} = F_n\left(1 + \frac{1}{k_0}\right)\mu_{pl} \tag{5.2}$$

The ploughing depths calculated using equations (2.2) and (3.2) is plotted in Fig. 4a and 4b as a function of the coating thickness for a hard coating and a soft coating and as a function of coating hardness with and without including the including the shear force $F_{sh}^{z}$ in the $z$ direction respectively. It can be seen from Fig. 4b, that $\mu_{sh}^{z}$ has a small contribution on the ploughing depth. The results obtained from the analytical model will be discussed further in comparison with the numerical MPM-ploughing model and ploughing experiments in section 4.1 and section 4.2 respectively. As the results shown in Figs. 3a and 4a are calculated over a large range of coating thickness $t$, the value of the fitting factor $k_1$ is varied (from 125 to 12.5) to avoid scaling effects and obtain smoother results.

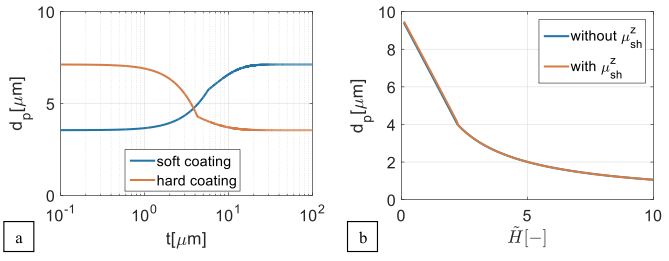


**Fig. 4.** Ploughing depth of rigid-plastic coated substrate by 1 mm diameter indenter at $F_n = 5$ N as a function of the (a) coating thickness $t$ for a soft coating ($\tilde{H} = 0.5$, $H_s = 900$MPa) and hard coating ($\tilde{H} = 2$, $H_s = 450$MPa) ($k_1 = 12.5$) and (b) relative coating hardness $\tilde{H}$($H_s = 450$MPa, $t = 4$ μm) with and without correction of $F_n$ using $\mu_{sh}^{z}$.

## 3. Experimental and computational method

The current section describes the set-up used to perform the ploughing experiments and the MPM-based ploughing simulation. The parameters of the material models and the interfacial friction models used in the ploughing simulations are also plotted and listed in this section.

### 3.1. Experimental method

The preparation of both the zinc block and the zinc coated specimen for the ploughing experiments is explained below. Also the ploughing experimental set-up is described.

#### 3.1.1. Preparation of specimen

The zinc coated steel sheets are prepared by hot dip galvanizing 210 mm long and 300 mm wide rectangular sheets in molten zinc bath. The surface of the (unrolled) zinc coating is characterized by dendritic growth and spangles (snowflake) formed during solidification of the molten zinc on surface of the steel sheet after hot dip galvanization as shown in Fig. 5a [53]. The surface roughness $R_a$ of the galvanized sheets is measured to be 0.5 μm. The mean thickness of the zinc coating is maintained within 20–55 μm by blowing off the excess zinc melt from the sheet using air knives. The thickness of the zinc coating on the steel is measured using the magnetic induction probe of Fisher's FMP 40 Dualscope.

Mirror polishing of rough galvanized steel sheets is done by hot mounting circular galvanized sheets of 46 mm diameter on 50 mm diameter bakelite disc. Polishing is done using an automatic polishing machine. The galvanized sheets were polished using a diamond suspension with 9 μm particle size at 30 N load, 150 rpm for 90 s. The fine polishing of the sheets was done using a (water-less) alcohol-based yellow lubricant, as the softness of zinc and its reaction with water can leave the coatings discoloured and with scratches. Firstly, the zinc coated surface was polished with a poly-crystalline diamond slurry suspension of 3 μm particle size at 25 N load, 150 rpm for 90 s. Then a diamond slurry suspension of 1 μm particle size was used at 20 N load, 150 rpm for 90 s. Finally, the sheets were polished using de-agglomerated gamma alumina powder of 0.05 μm particle size mixed with ethanol denatured with iso-propyl alcohol at 15 N and 150 rpm for 60 s. The polished sheet is shown in Fig. 6a where the grain boundaries can be clearly seen. The resulting mean surface roughness was 0.05 μm as shown in Fig. 6b. The resulting mean coating thickness of polished specimens was measured to be 15 μm. Zinc coated specimens with coating thickness of 10 μm were also obtained by increasing the polishing time and/or the applied load. To obtain zinc coated steel specimen with high coating thickness, given zinc coated steel sheets with coating thicknesses of 30, 40 and 55 μm were left unpolished to prevent any reduction in coating thickness.

For reducing the coating thickness, the duration and loads in the polishing steps were increased. Zinc coated specimens were also polished up to 10 and 15 μm coating thickness. Zinc coated samples with a mean coating thickness of 40 and 55 μm in an unpolished state were also used in the ploughing experiments as specimens high coating thickness. To simulate a very high zinc coating thickness, a zinc block was used. The rectangular zinc block was also mounted and polished to obtain a mean surface roughness of 0.05 μm as shown in Fig. 7.

#### 3.1.2. Experimental set-up

The ploughing experiments on zinc coated DX56 steel sheet and zinc block lubricated with Quaker FERROCOAT N6130 lubricant were done using the linear friction tester, shown in Fig. 8, with 3 repetitions. The linear friction tester consists of an XY linear positioning stage driven separately by actuators as shown in Fig. 8c. A horizontal beam supports the loading tip and moves the Z-stage using a linear and piezo actuator for coarse and fine displacement respectively while applying a normal

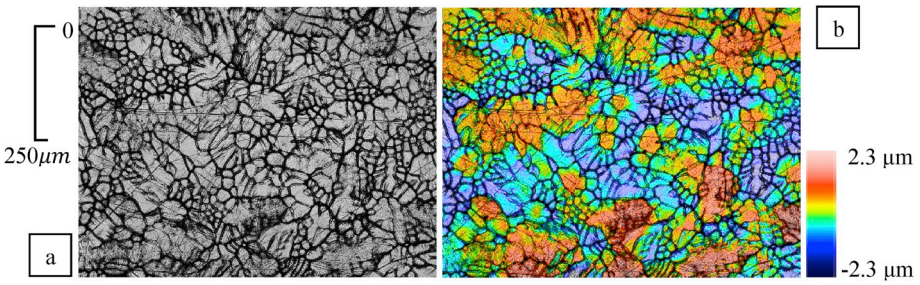


**Fig. 5.** Surface of mounted (zinc coated) galvanized sheet before polishing, (a) as seen under confocal microscope at 20x magnification with its (b) surface height profile, $R_a = 0.61\mu m$ and $R_q = 0.76\mu m$.

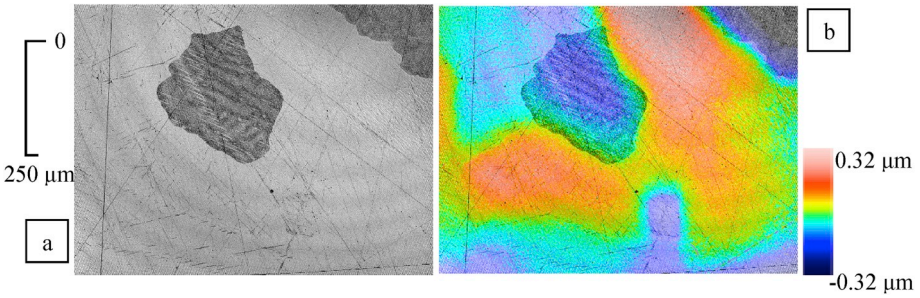


**Fig. 6.** Surface of mounted (zinc coated) polished galvanized sheet, (a) as seen under a confocal microscope at 20x magnification with its (b) surface height profile, $R_a = 0.08\ \mu m$ and $R_q = 0.11\mu m$.

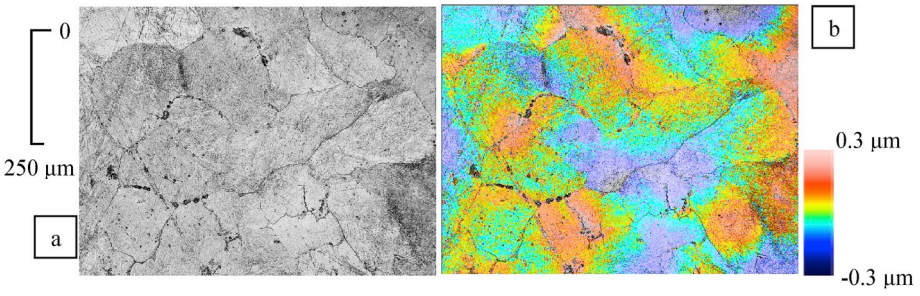


**Fig. 7.** Surface of mounted polished zinc block, (a) as seen under confocal microscope at 20x magnification with its (b) surface height profile, $R_a = 0.07\mu m$ and $R_q = 0.10\mu m$.

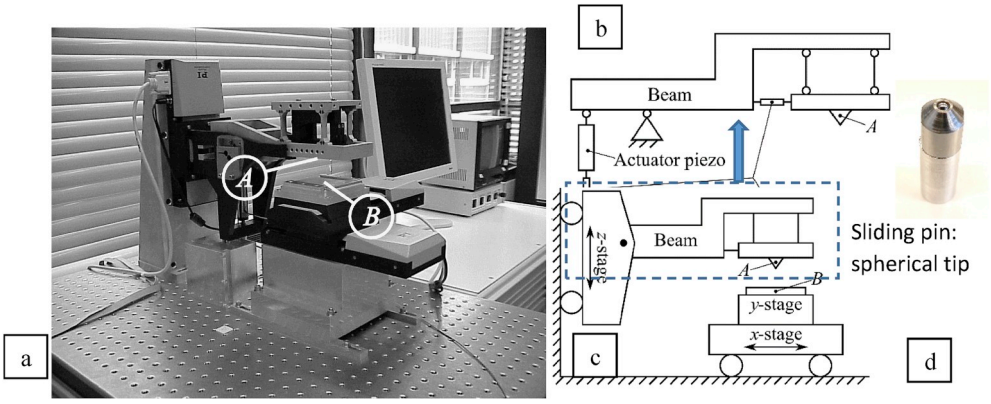


**Fig. 8.** (a) Linear friction tester for ploughing experiments with schematic of (b) A: loading set-up (c) B: sliding set up and (d) the indenter/pin with 3 mm diameter spherical tip.

load. The normal load is applied using a force controlled piezo actuator, connected by PID control loop feedback system, so the system can operate load-controlled. The friction forces are measured by a piezo sensor along the loading tip as shown in Fig. 8b. Spherical balls of 1 mm and 3 mm diameter were mounted on the pin holder as shown in Fig. 8d. In the experiments, the sliding distance was 10 mm and the sliding

velocity was set equal to 1 mm/s.

### 3.2. Computational method

The material point method (MPM), a particle-in-cell based modelling tool, has been used to simulate ploughing. The MPM-based ploughing model has been introduced and implemented successfully for ploughing of a steel sheet in Ref. [47]. In that paper, the model-set up, the material model and the interfacial friction model used in the MPM-based ploughing simulations have been elaborated. The governing equations used in material point method used in Ref. [47] has been further elaborated in Ref. [59]. Further, the parameters for the material model and the interfacial friction model have been listed using the data from tensile and compression tests, obtained from the supplier, the literature on bulk zinc and zinc coatings [44,45,54] and the experiments done for interfacial shear characterization in Ref. [48].

#### 3.2.1. Model set-up

The MPM-based ploughing model results are obtained by extrapolating and converging the results for decreasing particle/element sizes towards 0 μm size, where the size of the particles in coated-substrate is varied from 2.5, 5–10 μm and the size of the triangles in the indenter is varied from 5,10 and 20 μm. Indenters of radii 200, 500–1500 μm are used for analytical and experimental validation. The coating thickness is varied from 10-55 μm, comparable to the measured coating thickness of the zinc coated specimen. The particles in the coated-substrate are grouped in the half cylindrical domain of radius 200 μm and length 1 mm. A scratch length of 600 μm is made using a spherical indenter. Mass scaling is used to vary the time step in the system. The values of mass scaling factor $m_s$ and sliding velocity of the indenter $v_i$ are varied within certain ranges resulting in stable computations while not affecting the model results. Further $v_i = 0.1$m/s and $m_s = 10^6$ are chosen to obtain fast and stable computations. Table 1 list the MPM model set-up parameters. Fig. 9 shows the MPM-ploughing model set-up.

The material model computes the total stress as a sum of the hydrostatic stress and the deviatoric stress. The hydrostatic stress is computed using a linear equation of state as given in equation (6.1). The bulk modulus $K$ is obtained from the Young's modulus $E$ and the Poissons ratio $\nu$ while the hydrostatic strain is obtained from the volumetric change M and identity matrix $I$. The deviatoric stress is obtained by updating the flow stress using a radial return plasticity algorithm [47]. Assuming, adiabatic conditions, the heat generated $\Delta q$ due to plastic deformation results in a temperature change $\Delta T$ which is calculated in equation (6.2) using the specific heat capacity $c_p$ and the mass of the particle $m = \rho V$ (material density $\rho$ and cell volume $V$). The heat transfer is calculated using thermal conductivity $\kappa_t$. The parameters for heat transfer in zinc and steel are listed in Tables 3 and 4.

$$\sigma_h = KMI, \text{ where } K = \frac{E}{3(1-2\nu)} \tag{6.1}$$

**Table 1**
MPM ploughing model parameters.

| Parameters | Symbol | Values/expression |
|---|---|---|
| Rigid spherical indenter radii | $R_i$ | 0.2, 0.5 and 1.5 mm |
| Semi-cylindrical substrate radius | $R_s$ | 0.2 mm |
| Sliding distance of indenter | $l$ | 0.6 mm |
| Semi-cylindrical substrate length | $l_s$ | 1 mm |
| Coating thickness | $t$ | 15 and 30 μm |
| MPM particle cell size | $r_p$ | 2.5, 5 and 10 μm |
| Indenter's mesh element size | $r_t$ | 5, 10 and 20 μm |
| Sliding velocity of indenter | $v_i$ | 0.1 mm/s |
| Mass scaling factor | $m_s$ | $10^6$ |

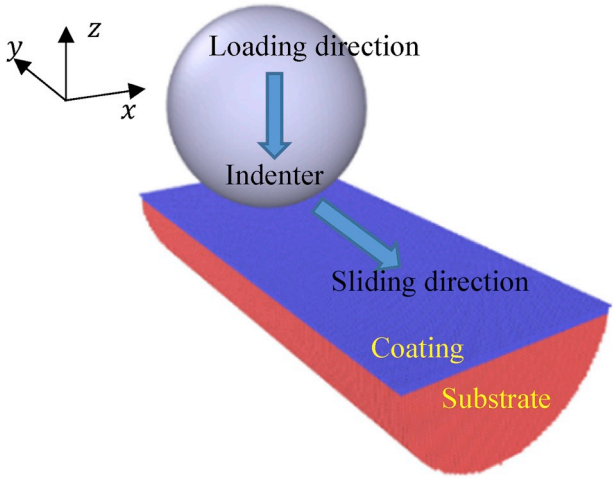


**Fig. 9.** MPM simulation of an spherical indenter (asperity) with radius 0.2 mm ploughing through a coated-substrate along sliding $x$-direction.

**Table 2**
Material parameters for rigid-plastic material.

| Parameters | Symbol | Value/expression |
|---|---|---|
| Elastic modulus of the substrate | $E_s$ | 210 GPa |
| Poisson's ratio (coating and substrate) | $\nu$ | 0.3 |
| Elastic modulus of the coating | $E_c$ | 80 GPa |
| Reference hardness of the coating | $H_{0_c}$ | 225/450 MPa |
| Reference hardness of the substrate | $H_{0_s}$ | 450/900 MPa |
| Reference coating thickness | $t_0$ | 25 μm |
| Relative hardness of coating | $\bar{H}$ | 0.1 – 10 |
| Coating thickness | $t$ | 0 – 200μm |
| Interfacial shear stress | $\tau_{sh}$ | $H/3\sqrt{3}$ |

**Table 3**
Parameters for DX56 steel substrate [47].

| Parameters | Symbols | Value |
|---|---|---|
| Heat transfer | | |
| Material density | $\rho$ | 7850 kg/m$^3$ |
| Specific heat capacity | $c_p$ | 502 J/(kg K) |
| Thermal conductivity | $\kappa_t$ | 50 W/(m K) |
| Equation of state | | |
| Young's modulus | $E$ | 210 GPa |
| Poisson's ratio | $\nu$ | 0.3 |
| Material model | | |
| Initial static stress | $\sigma_{f0}$ | 82.988 MPa |
| Stress increment parameter | $d\sigma_m$ | 279.436 MPa |
| Linear hardening parameter | $\beta$ | 0.482 |
| Remobilization parameter | $\omega$ | 6.690 |
| Strain hardening exponent | c | 0.5 |
| Initial strain | $\varepsilon_0$ | 0.005 |
| Initial strain rate | $\dot{\varepsilon}_0$ | $10^8$ s$^{-1}$ |
| Maximum dynamic stress | $\sigma_{v0}$ | 1000 MPa |
| Dynamic stress power | $m$ | 3.182 |
| Activation energy | $\Delta G_0$ | 0.8 |
| Boltzmann's constant | $k$ | $8.617 \times 10^{-5}$ eV |

**Table 4**
Parameters for zinc [44,45,54].

| Parameters | Symbols | Value |
|---|---|---|
| Heat transfer | | |
| Material density | $\rho$ | 7140 kg/m$^3$ |
| Specific heat capacity | $c_p$ | 377 J/(kg K) |
| Thermal conductivity | $\kappa_t$ | 116 W/(m K) |
| Equation of state (bulk) | | |
| Young's modulus | $E$ | 108 GPa |
| Poisson's ratio | $\nu$ | 0.25 |
| Material model (bulk) | | |
| Initial yield stress | $A$ | 82.51 MPa |
| Strain hardening exponent | $p$ | 0.1786 |
| Strain hardening constant | $B$ | 288.34 |
| Strain rate hardening constant | $C$ | 0.0202 |
| Reference strain rate | $\dot{\varepsilon}_0$ | 1s$^{-1}$ |
| Thermal softening constant | $q$ | 0.843 |
| Reference temperature | $T_0$ | 298 K |
| Melting point temperature | $T_m$ | 692.68 K |
| Equation of state (coating) | | |
| Young's modulus | $E$ | 80 GPa |
| Poisson's ratio | $\nu$ | 0.3 |
| Material model (coating) | | |
| Initial yield stress | $\sigma_{y_0}$ | 85 MPa |
| Strain hardening exponent | $n$ | 0.14 |

$$\Delta T = \frac{\Delta q}{mc_p} \tag{6.2}$$

The flow stress $\sigma_y$ is taken as constant for a rigid-plastic material. In the model, the flow stress is computed for materials using physically based material models. The isothermal Bergström van Liempt hardening relation [55], modified by Vegter for sheet metal forming processes [56], is used for the DX56 steel substrate where the flow stress $\sigma_y^{\mathrm{BL}}$ is decomposed into a static-strain hardening stress $\sigma_{wh}$ and dynamic stress $\sigma_{dyn}$. It takes into account the strain $\varepsilon$, strain-rate $\dot{\varepsilon}$ and thermal (temperature) $T$ effects as shown in equation (7.1). The Bergström van Liempt material model (equation (7.1)) parameters for the DX56 steel sheet are listed in Table 3 [47]. The Johnson-Cook material model is used for modelling the flow stress $\sigma_y^{JC}$ of the bulk zinc specimen [57] as shown in equation (7.2) where $\varepsilon$ is strain, $\dot{\varepsilon}$ is strain-rate and $T$ is temperature. The flow stress $\sigma_y^S$ for the zinc coating is computed from the initial yield stress $\sigma_{y_0}$ using the material model in equation (7.3). The model is taken from Refs. [43,44], and has similarities with the Swift strain hardening law [58]. Table 4 lists the material model parameters for bulk zinc and zinc coating, given in equations (7.2) and (7.3).

$$\sigma_y^{\mathrm{BL}} = \sigma_{wh} + \sigma_{dyn}$$
$$= \sigma_{f0} + d\sigma_m(\beta(\varepsilon+\varepsilon_0) + \{1-\exp[-\omega(\varepsilon+\varepsilon_0)]\}^c) + \sigma_{y0}\left(1+\frac{kT}{\Delta G_0}\ln\frac{\dot{\varepsilon}}{\dot{\varepsilon}_0}\right)^m \tag{7.1}$$

$$\sigma_y^{JC} = (A+B\varepsilon^p)\left(1+C\ln\frac{\dot{\varepsilon}}{\dot{\varepsilon}_0}\right)\left(1-\left(\frac{T-T_0}{T_m-T_0}\right)^q\right) \tag{7.2}$$

$$\sigma_y^S = \sigma_{y_0}\left(1+\frac{E}{\sigma_{y_0}}\varepsilon\right)^n \tag{7.3}$$

The interfacial friction algorithm is used to calculate the friction force due to shearing of the interface as the product of the interfacial shear strength $\tau_{bl}$ and contact area $A_c$. For rigid-plastic materials, the interfacial shear strength can be given as a fraction $f$of the bulk shear strength $\kappa$ in equation (8.1) (model parameters listed in Table 2 and used in section 4.1). The boundary-layer shear strength at the interface of the indenter and the metallic coating/substrate (lubricated) is given as a function of the nominal contact pressure $\overline{P}$, sliding velocity $v_i$ and the contact temperature $T_0$ in equation (8.2) [43], where, $C_0$ is the proportionality constant, $n_p$ is the pressure exponent, $n_v$ is the velocity exponent and $n_T$ is the temperature exponent, obtained by fitting experimental data. For a constant $v_i$ and $T_0$, a power-law relationship between $\tau_{bl}$ and $\overline{P}$ can be deduced in equation (8.3). This interfacial friction model is used in ploughing simulation of zinc coated steel in section 4.2 (model parameters are given in Table 5).

$$\tau_{bl} = f\kappa \tag{8.1}$$

$$\tau_{bl} = C_0\overline{P}^{n_p} v_i^{n_v} \exp -\frac{n_T}{T_0} \tag{8.2}$$

$$\tau_{bl} = C_p\overline{P}^{n_p} \tag{8.3}$$

### 3.2.2. Model parameters

The material model parameters for bulk specimens of DX56 steel sheets are obtained by uniaxial tensile tests. Tensile tests are done at various strain rates and temperatures up to a true strain of 1. The resulting stress-strain curves are fitted with equation (7.3) to obtain the model parameters, listed in Table 3. The strain hardening parameters ($A$, $B$ and $p$) of the zinc block are obtained by fitting the stress-strain data from the uniaxial compression tests perpendicular to the rolling plane with equation (7.2). The strain rate hardening and thermal softening parameters ($C$ and $q$) are obtained by fitting the results from Kolsky bar experiments done on commercially pure zinc in Ref. [54] with equation (7.2). The material model parameters for the zinc coating on steel in Refs. [43,44] are obtained from the load–depth curves of nanoindention experiments measured on various zinc grains in Ref. [45]. The material parameters for bulk zinc and the zinc coating are listed in Table 4.

The true stress-strain curves of the DX56 steel, bulk zinc and zinc coating are plotted in Fig. 10a [44,45]. The DX56 steel shows highest flow stress (hardness) compared to both the bulk zinc and zinc coating. The pure zinc block shows higher strain hardening, although low yield strength compared to the zinc coating. The interfacial friction model parameters for Quaker lubricated zinc coated steel sheet and uncoated steel sheet have been obtained by performing boundary layer shear experiments in a linear friction tester [48]. Likewise, the boundary layer shear stress of the Quaker lubricated steel sheet and Quaker lubricated zinc coated steel sheet are plotted as a function of the applied nominal pressure in Fig. 10b. The boundary layer shear strength results are used to calibrate the interfacial friction model given in equation (8.2). The model parameters obtained are listed in Table 5. The boundary layers at the interface of the zinc coating and the sliding pin have a lower shear strength compared to those formed at the interface of the DX56 steel sheet and the sliding pin.

The material parameters, listed in Table 2 are for rigid-plastic material behaviour. The relative hardness of the coating to the substrate $\breve{H} = H_c/H_s$ is varied from 0.1 to10 to study the effect of coating hardness

**Table 5**
Interfacial friction model parameters [48].

| Parameters | Symbols | Value |
|---|---|---|
| Quaker lubricated DX56 steel sheet | | |
| Pressure constant | $C_p$ | 1.34 |
| Pressure exponent | $n_p$ | 0.88 |
| Quaker lubricated Zinc coated steel sheet | | |
| Pressure constant | $C_p$ | 0.32 |
| Pressure exponent | $n_p$ | 0.95 |

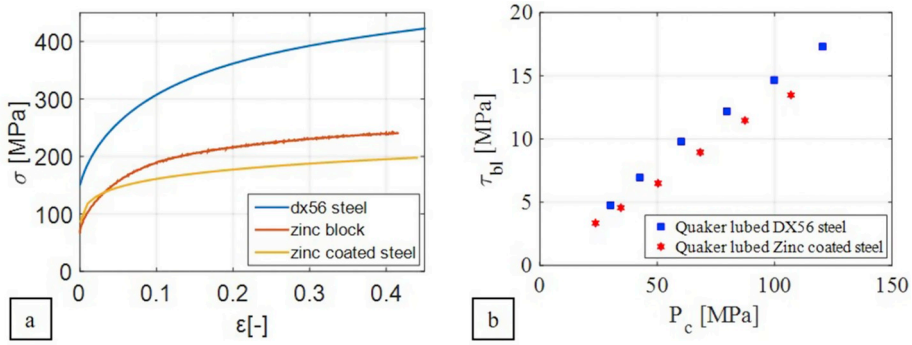


**Fig. 10.** Comparison of (a) the true flow stress-strain curves for DX56 steel sheet, zinc coated steel sheet and zinc block obtained by uniaxial compression test and (b) of the boundary layer shear stress against applied nominal pressure of DX56 steel sheet and zinc coated steel sheet lubricated with Quaker FERROCOAT N136 lubricant [48].

on ploughing friction and ploughing depth. The coating thickness $t$ is varied from 0 (uncoated substrate) to ∞ (bulk coating) to study the effect of coating thickness on ploughing friction and ploughing depth. To simulate rigid-plastic behaviour, hardness is taken as $H = 3\sigma_y$ [51] and shear strength of the bulk is taken as $\kappa = \sigma_y/\sqrt{3}$ [10]. The interfacial friction factor is taken to be $f = 1$ assuming a very clean surface. A high value of (maximum) interfacial shear in the analytical study can help highlight its effect on the overall ploughing friction. The interfacial friction model given in equation (8.3) is used to determine the interfacial shear strength.

## 4. Results and discussion

The coefficient of friction and ploughing depths obtained from the MPM-based ploughing simulations of the coated systems have been compared with those obtained from the analytical model in section 2. The coating thickness and relative material hardness has been varied to study their effect on friction and ploughing depths for rigid-plastic material behaviour. Ploughing experiments have been performed on bulk zinc and zinc coatings on a steel substrate over a range of coating thicknesses and applied loads using spherical indenters of two different sizes. The coefficient of friction and the ploughing depths obtained from the experiments are used to validate the results obtained from the MPM-based ploughing model and thereby to study the effects of applied load, indenter size, coating thickness and substrate material properties on the ploughing behaviour of (soft) coated system such as galvanized steel. The MPM results obtained for particle sizes of 5 and 10 μm are extrapolated to converge to infinitesimal particle sizes.

### 4.1. Analytical validation of the MPM-based ploughing model

In the following, the ploughing depths and the coefficient of friction obtained from the theory given in section 2 has been plotted and compared with those obtained from the ploughing simulations of rigid-plastic coated-substrates in section 4.1.1 and 4.1.2 respectively. The effects of relative hardness of the coating with respect to the substrate $\tilde{H}$ and the coating thickness $t$ on the coefficient of friction and the ploughing depths have been studied. The material parameters used in the MPM-simulations of the rigid-plastic coated-substrates to be compared with the analytical model in this section are listed in Table 2.

The ploughing depth and coefficient of friction, are obtained for the ploughing simulations utilize a 0.4 mm diameter indenter at 3 N load. A coating thickness of $t = 25$μm is taken in the first study where the relative hardness of the coating $\tilde{H}$ is varied from 0.1 to 10 and the interfacial shear strength is varied for two different cases. In the first case, the interfacial shear strength of the coating $\tau_c$ and the substrate $\tau_s$ is kept constant at $H_0/k_0$ where $H_0 = 450$MPa and $k_0 = 3\sqrt{3}$. In the second case, the interfacial shear strength of the coating and the substrate is taken as per $\tau = H/k_0$ where $H = H_s$ for the substrate and $H = H_c$ for the coating. In the second study, the coating thickness is varied from 0 μm for uncoated substrate to 200 μm for the coating material as bulk. The relative coating hardness is varied for two different cases. In first case, $\tilde{H} = 0.5$ ($H_c = 450$ MPa, $H_s = 900$MPa) and in the second case, $\tilde{H} = 2$($H_s = 900$ MPa, $H_c = 450$MPa).

#### 4.1.1. Comparison of ploughing depth

The total ploughing depth obtained from the ploughing simulations is compared with that obtained by the analytical model in Fig. 11 using equations (2.2) and (3.2) which calculate the ploughing depths with and without considering the interfacial friction force in the $z$ direction. The ploughing depths obtained by the analytical model agree well for those obtained from the ploughing simulations for both studies.

In the first study, where the relative hardness $\tilde{H}$ is varied from 0.1 to 10, the ploughing depths obtained using the analytical model and the MPM simulations decrease with $\tilde{H}$ and are shown to agree for $\tilde{H} \geq 0.5$ in Fig. 11a. For low values of $\tilde{H}$ (coating hardness), the ploughing depths obtained from the MPM model exceed those calculated by the analytical model. Also for low values of $\tilde{H}$, the indenter penetrates more into the coating and the simulated ploughing depths exceed the coating thickness resulting in the wear of the coating material as shown in the corresponding MPM ploughing simulations in Fig. 12a. The coating material piles up in front of the indenter as layers and wears out which can be related to degradation mechanisms such as peeling and delamination of thin soft coatings, as also shown in Ref. [22]. The results in Fig. 11a show that ploughing depth $d_p$ is not affected by the interfacial shear strength.

In the second study, the total ploughing depths for a hard coating ($\tilde{H} = 2$) and for a soft coating ($\tilde{H} = 0.5$) are studied as a function of the coating thickness $t$ as shown in Fig. 11b. The ploughing depths obtained from the MPM ploughing simulations agree well with those obtained from the analytical model. The ploughing depth for the soft coated system increases with coating thickness, as the effective hardness of the soft coated system decreases with the increase in coating thickness. Consequently, the ploughing depth for the hard coated system decreases with coating thickness as the effective hardness increases with the coating thickness (equation (1)). The slope of the ploughing depth plots changes at a coating thickness $t_c = 5.75$μm for the soft coating and $t_c = 4.3$μm for the hard coating where $d_p = t$ after which increase in $t$ results in transition of the contact of the indenter from both the substrate and the coating to the coating only. So, the ploughing depths are calculated accurately by MPM for all cases.

#### 4.1.2. Comparison of coefficient of friction

The overall coefficient of friction $\mu$, obtained from the MPM ploughing simulations is also compared with the values obtained by the

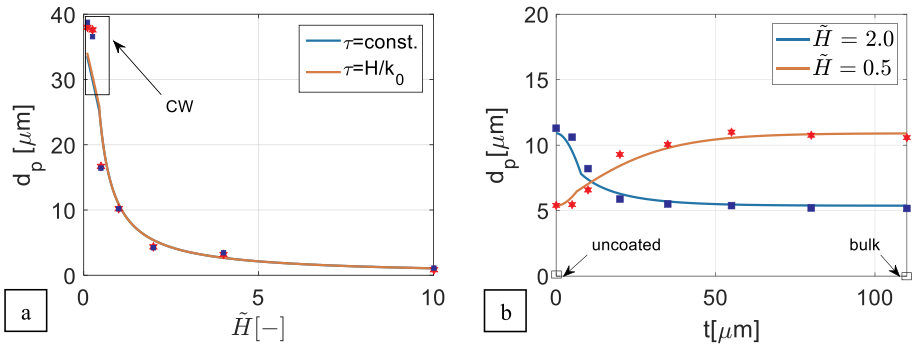


**Fig. 11.** Simulated ploughing of rigid-plastic coated substrate by 0.4 mm diameter ball at 3 N load. (a) Effect of relative coating hardness $\tilde{H}(t = 25\ \mu m)$ on the total ploughing depth with a constant interfacial shear and with interfacial shear $\tau = H/k_0$. (b) Effect of coating thickness on the total ploughing depth for a hard coating ($\tilde{H} = 2$) and a soft coating ($\tilde{H} = 0.5$). (Marks: MPM model, Lines: Analytical model). CW: Coating wear/degradation.

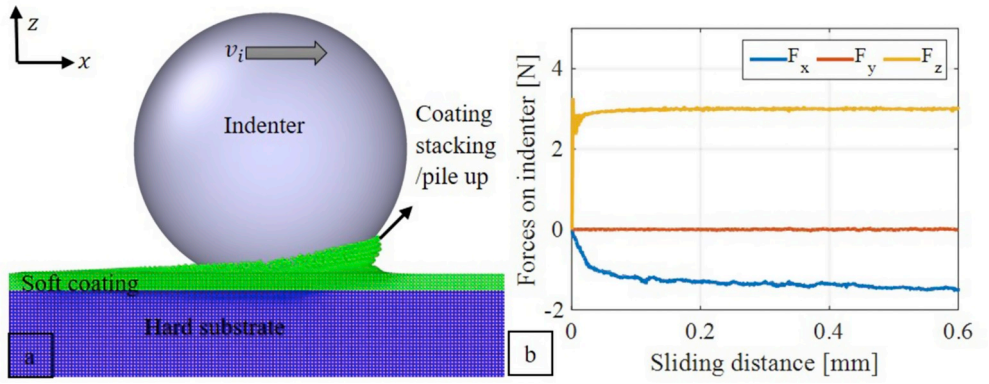


**Fig. 12.** Ploughing of a spherical indenter through a soft coating on a hard substrate ($\tilde{H} = 0.25,\ t = 25\ \mu m$) resulting in pile up, stacking and eventual peeling off of the coating. (b) The corresponding plot of components forces acting on the indenter.

analytical model using equation (4.2) which combines $\mu_{pl}$ and $\mu_{sh}$ for a coated substrate. The results are shown to agree well in both the case studies depicted in Fig. 13. The mean coefficient of friction is calculated from the friction plots given in Fig. 12b. The steady increase in friction force can be seen over the sliding distance in Fig. 12b which corresponds to the piling up of material in front of the coating as shown in Fig. 12a.

The calculated coefficient of friction plotted against $\tilde{H}$for a constant interfacial shear stress (Fig. 13a) shows a good agreement with the simulated coefficient of friction. The ploughing depth at $\tilde{H} = 0.46$ corresponds to the coating thickness $t = 25\mu m$ as shown in Fig. 11a. Hence, at lower $\tilde{H}$ and for $d_p > t$, there is coating wear, resulting in the difference in friction computed by the MPM model and the analytical ploughing model. As $\tau_{sh_c} = \tau_{sh_s}$ is constant, and $d_p$ and consequently $A_{pl}$ and $A_{sh}$ decrease with $\tilde{H}$, thereby decreasing $\mu_{pl}$ and $\mu_{sh}$. However in the case where $\tau_{sh_c} = H_c/k_0$, $\mu_{sh} = \tau_{sh_c} A_{sh}$ increases with as $H_c(\tilde{H})$, in spite of the decrease in $A_{pl}$ and $A_{sh}$. Therefore the simulated coefficient of friction increases with $\tilde{H}$ is also shown in Fig. 3c, and agrees with the simulated coefficient of friction.

The coefficient of friction has been plotted as a function of the coating thickness $t$ for a hard coating ($\tilde{H} = 2$) and a soft coating ($\tilde{H} = 0.5$) in Fig. 13b. The coefficient of friction obtained from the MPM simulations agrees well with the values obtained from the analytical model. For a low coating thickness, the indenter is in contact with both the coating and the substrate. In Fig. 13b, $\mu$ is shown to initially increase

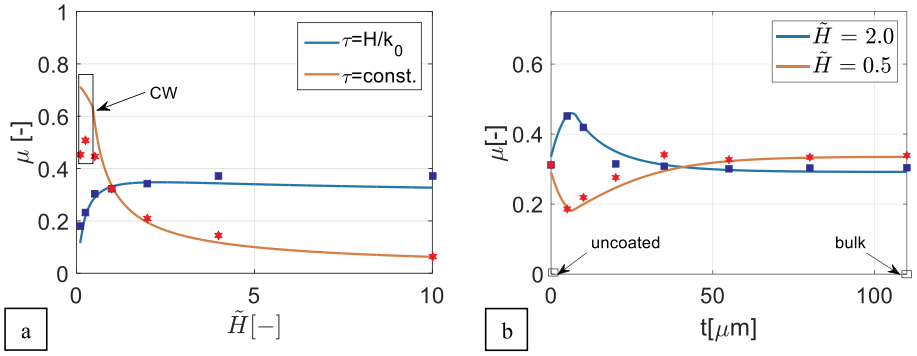


**Fig. 13.** Simulated ploughing of rigid-plastic coated substrate by 0.4 mm diameter ball at 3 N load. (a) Effect of relative coating hardness ($t = 25\ \mu m$) on the overall coefficient of friction with a constant interfacial shear and with interfacial shear $\tau = H/k_0$. (b) Effect of coating thickness on the total ploughing depth for a hard coating ($\tilde{H} = 2$) and a soft coating ($\tilde{H} = 0.5$). ($r = 200\ \mu m,\ k_1 = 12.5$) (Marks: MPM model, Lines: Analytical model). CW: Coating wear/degradation.

and then decrease with $t$ for the hard coating. The initial increase in $\mu$ corresponds to the increase in contact area due to increase of the (hard) coating thickness which require more friction force to shear and plough. However once the indenter is in contact with the coating only ($t > 7.8$ μm), the coefficient of friction plot follows the ploughing depth plot, and decreases with increase in $t$ for the hard coating. Therefore, with the same analogy, the coefficient of friction first decreases and then increases ($t > 6.5$ μm) with coating thickness for a soft coating. The plots in Fig. 13b resembles the coefficient of friction versus thickness plots in Fig. 3a and 3b. A fitting factor of $k_1 = 12.5$ is used to calculate $H_{cs}$ for $r = 0.2$mm. It can be concluded that the MPM accurately predicts the coefficient of friction for ploughing in a coated substrate.

### 4.2. Experimental validation of ploughing friction and depths

The friction and ploughing depths are obtained from the MPM-based ploughing model over a range of applied loads (1–46 N) and indenter sizes of 1 mm and 3 mm. The coefficient of friction and ploughing depths were calculated for MPM particle sizes of 2.5, 5 and 10 μm and extrapolated to 0 μm to obtain a resolution independent result. The plots for the friction force and the ploughed profile obtained from the ploughing simulation are compared with those obtained from the ploughing experiments. The material parameters listed in Tables 3–5 are used in the MPM ploughing model in this section. So the actual material behaviour has been implemented.

#### 4.2.1. Comparison of ploughed profile

The height profile of the ploughed surface in the sliding $xy$ plane obtained from the ploughing experiments and the MPM simulations are shown in Fig. 14a and 14b respectively. The ploughed profiles are plotted over the cross-section ($yz$ plane) in Fig. 14c. The MPM particles along the cross-section of the wear track (see Fig. 14d) were grouped and their positions at the end of the simulation were plotted in Fig. 14d. The cross-section of the ploughed profile obtained from both the ploughing experiments and the MPM simulations showed good agreement in Fig. 14c. The total ploughing depth $d_p$ is calculated as the sum of the groove depth $d_g$ and the pile-up height $h_{pu}$ in Fig. 14c.

The total ploughing depths obtained from the ploughing experiments with uncoated steel sheet [47] and with zinc blocks, both lubricated by Quaker lubricant and ploughed by a 1 mm diameter ball, were compared with the corresponding simulated (MPM) ploughing depths and found to be in good agreement (see Fig. 15). The zinc block having a lower yield stress compared to the DX56 steel sheet (see Fig. 10a) resulted in a higher ploughing depth for all the loads. The ploughing depth for the zinc blocks also increased faster than that of the DX56 steel sheets due to the lower strain hardening of the zinc block at high loads compared to the DX56 steel sheet (see Fig. 10, Table 3 and Table 4). Having validated the ploughing depth for bulk zinc and steel, the numerically calculated

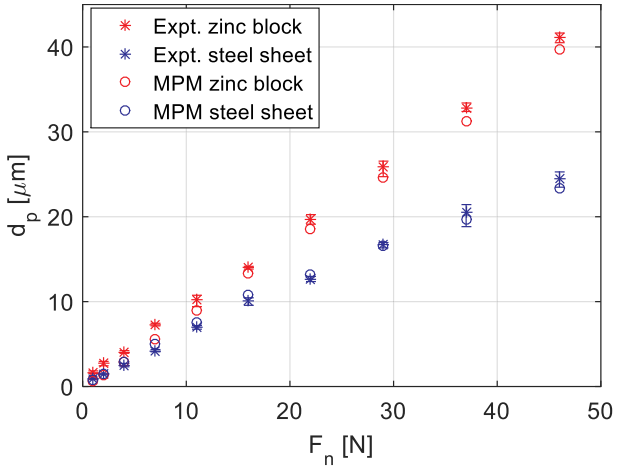


**Fig. 15.** Comparison of the ploughing depths obtained from MPM model and ploughing experiments on Quaker lubricated zinc block and DX56 steel sheet by a 1 mm diameter ball [48]. (MPM model parameters: Tables 3–5).

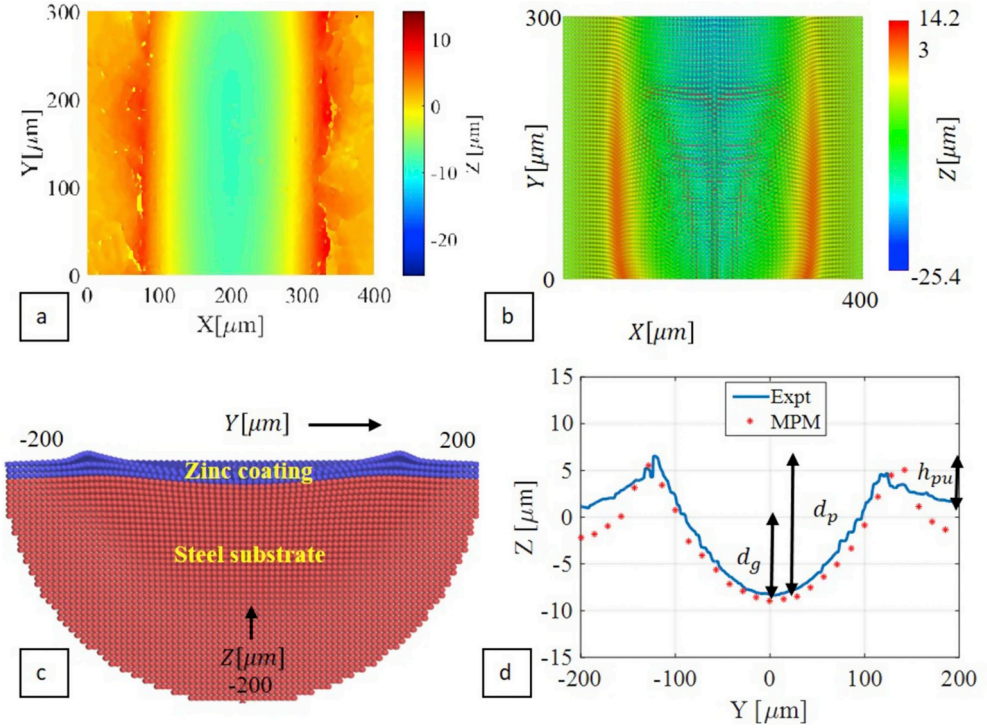


**Fig. 14.** Surface profile of zinc coating on steel ploughed at 22 N load by 1 mm dia. sphere in (a) ploughing experiments as seen using confocal microscope at 20x magnification and from (b) MPM-simulations as seen using OVITO visualization tool. (c) Comparision of the ploughed cross-section obtained from MPM-simulation and experiments by 1 mm dia. ball at 22 N load. (d) Cross-section of the zinc coated specimen during ploughing. (MPM model parameters: Tables 3–5).

ploughing depths will be also validated using zinc coated steel sheet.

The total ploughing depth obtained from the ploughing experiments and simulations on the zinc coated steel sheet for a load range of 1–46 N were compared for spherical indenters of 1 mm and 3 mm diameters and found to agree well as shown in Fig. 16. It is obvious that the larger 3 mm diameter indenter penetrates less compared to the 1 mm indenter owing to its larger contact area to carry the applied load.

Ploughing experiments and MPM simulations were also done for zinc coated steel sheets with a coating thickness ranging from 0-55 μm including the zinc block (bulk zinc). The ploughed profile of the zinc coated steel sheets was compared with the ploughed profile of the zinc block at the zinc surface and at 15 μm beneath the surface, see Fig. 17. For a zinc coated steel sheet with 15 μm coating thickness, the deformation of the (surface of the steel substrate) bulk steel is significantly lower than the bulk zinc due to its higher hardness as shown in Fig. 17a and 17b. Also, the higher hardness of the steel substrate results in a lower ploughing depth at the surface of the zinc coating as compared to that of the zinc block as shown in Fig. 17a and 17b.

The differences in the ploughing depths obtained from experiments with steel sheet, zinc coated steel sheet and the zinc block are summarised over loads ranging from 1-46 N in Fig. 18a. As the thickness of the zinc coating is increased from 10 to 15, 30, 40 and 55 μm, the ploughing depths are also shown to increase for three different loads in Fig. 18b. The increase in ploughing depth with coating thickness is due to the decrease in the effective hardness for the soft zinc coated system with increase in coating thickness (see equation (1)). The rate of increase in ploughing depth with respect to the coating thickness increases with increase in the applied load. The MPM simulations have a larger increase in ploughing depth compared to that of the experiments with coating thickness above 20 μm, as shown in Fig. 18b. The lower penetration depths obtained from the ploughing experiments for large coating thickness (30, 40 and 55 μm) can be explained by the rougher surface of thicker (unpolished) zinc coatings which could result in higher surface hardness of the zinc coatings. Further the yield strength of the zinc coating used in the MPM simulations is measured by Nano-indentation for a coating thickness of 10 μm [45]. For higher coating thickness, the size and orientation of the zinc grains could have significant effect on the measured yield strength and hardness. The mechanical properties of the thicker zinc coatings are unknown in the current analysis to be used in the MPM model.

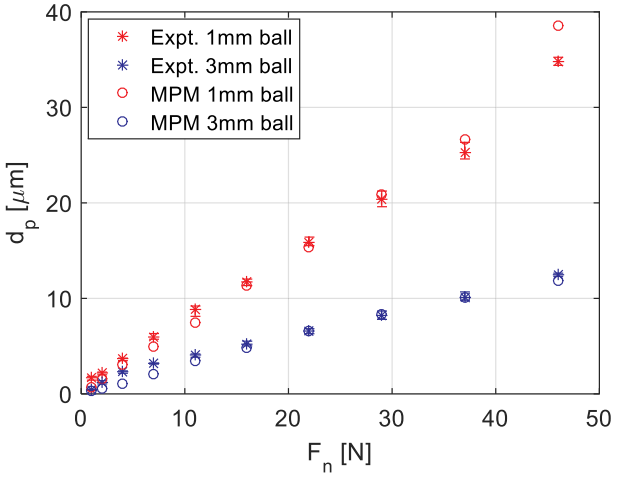


**Fig. 16.** Ploughing depths for load controlled test carried out with indenters of diameter 1 mm and 3 mm on lubricated zinc coated steel sheet (zinc coating thickness of 15 μm) with the linear sliding friction tester and MPM-ploughing model that includes the material model parameters from Tables 3 and 4 and interfacial friction model parameters in Table 5. (MPM model parameters: Tables 3–5).

*4.2.2. Comparison of coefficient of friction*

The forces acting on the indenter were plotted over the sliding distance as obtained from the ploughing experiments and simulations in Fig. 19. The pin was slid over a distance of 0.6 mm in the MPM simulations. The friction force $F_x$ due to ploughing in $x$ direction is divided by the normal force $F_z$ to obtain the overall coefficient of friction $\mu$. The average coefficient of friction was measured during steady state from 3 mm to 9 mm sliding distance in the ploughing experiments and from 0.3 mm to 0.6 mm sliding distance in MPM simulations.

The coefficient of friction is obtained for the MPM ploughing simulations on the zinc block and the DX56 steel substrate lubricated with Quaker oil by a 1 mm diameter ball is shown to be in good agreement over the load range of 1–46 N in Fig. 20. The coefficient of friction for ploughing of the zinc block is slightly higher than for the DX56 steel sheet at normal loads larger than 7 N. The higher coefficient of friction results from the larger plastic deformation of the bulk zinc during ploughing as can be seen from the higher ploughing depths for the bulk zinc in Fig. 15. However, in spite of a large difference in the ploughing depths between bulk zinc and steel sheet, resulting in a large component of coefficient of friction $\mu_{pl}$, the difference in the overall coefficient of friction is minimized. This is due to the large contribution of the coefficient of friction due to interfacial shear $\mu_{sh}$ to the overall $\mu$ [48], where the boundary layer shear strength $\tau_{bl}$ of lubricated zinc is also lower than that of the lubricated steel sheet (see Fig. 10b). The coefficient of friction at lower loads is higher for the ploughing experiments compared to the MPM simulation due to the possible asperity interlocking at low $d_p$.

The mean coefficient of friction obtained from both ploughing experiments and MPM simulations was plotted over a range of loads (1–46 N) for spherical indenters of 1 mm and 3 mm diameters sliding over zinc coated steel sheet in Fig. 21. The coefficient of friction obtained from the MPM ploughing model is very close to that obtained from the ploughing experiments. The coefficient of friction obtained for ploughing with 1 mm diameter ball increases steadily with the applied load range of 1–46 N. However, as the diameter of the indenter is increased to 3 mm, the coefficient of friction drops significantly compared to ploughing with 1 mm ball. The increase in indenter size reduces the penetration of the indenter into the coating required to balance the applied load. The effective hardness of the coated system in response to penetration by an indenter with larger radius is also higher as can be deduced from equation (1) [50]. Furthermore, the increase in indenter size also increases the relative contribution of interfacial shear strength to the coefficient of friction as shown in Ref. [48]. Consequently, the coefficient of friction due to interfacial shear reduces with increase in applied load. However, for large indenters although the coefficient of friction due to ploughing increases with load. The later counterbalances the decreasing coefficient of friction due to interfacial shear. This results in almost constant overall coefficient of friction over the range of applied loads.

*Effect of asperity size and load on ploughing friction by an experimentally fit analytical model.* The effect of asperity size on ploughing friction is explained below using the analytical ploughing model and power law curve fitting of experimental data in equations (9.1)-(9.2) for their mathematical simplicity. The ploughing depth here is taken to be less than the coating thickness. The relationship between the ploughing depth and applied load for the 1 mm and 3 mm diameter indenters is obtained by power law fitting of Fig. 16. Taking $d_p = a_1 F_n^{x_1}$, we have $a_1 = 8.6 \times 10^{-6}$, $x_1 = 0.95$ for 1 mm dia. ball and $a_1 = 4.7 \times 10^{-6}$, $x_1 = 0.85$ for 3 mm dia. ball. By curve fitting the relationship between $A_{yz}$ and the ploughing depth $d_p$ from equation 2.3 to a power law $A_{yz} = b_1 d_p^{y_1}$, the coefficients $b_1 = 1.51$, $y_1 = 0.96$ and $b_1 = 0.15$, $y_1 = 1.5$ are obtained for 1 mm and 3 mm dia. balls respectively. Assuming a constant hardness $H_c = 3\sigma_{y_0}$ where $\sigma_{y_0}$ for zinc is taken 85 MPa [46], an analytical expression of $\mu_{pl}$ in given in terms of $F_n$ in equation (9.1). By curve fitting the relationship between $A_{xy}$ a nd the ploughing depth $d_p$ from equation 2.2 to a power law $A_{yz} = c_1 d_p^{z_1}$, the coefficients $c_1$ =

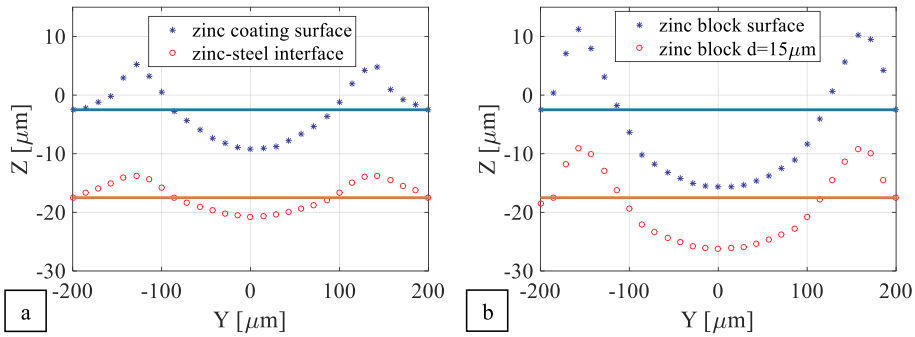


**Fig. 17.** Comparison of deformation in the ploughed specimen (ploughed cross-section profile) at the surface (blue) and the interface 15 μm depth (red) (a) in presence of 15 μm zinc coating on steel substrate and (b) with pure zinc block under 22 N load by 1 mm diameter indenter (MPM model parameters given: Tables 3–5). (For interpretation of the references to colour in this figure legend, the reader is referred to the Web version of this article.)

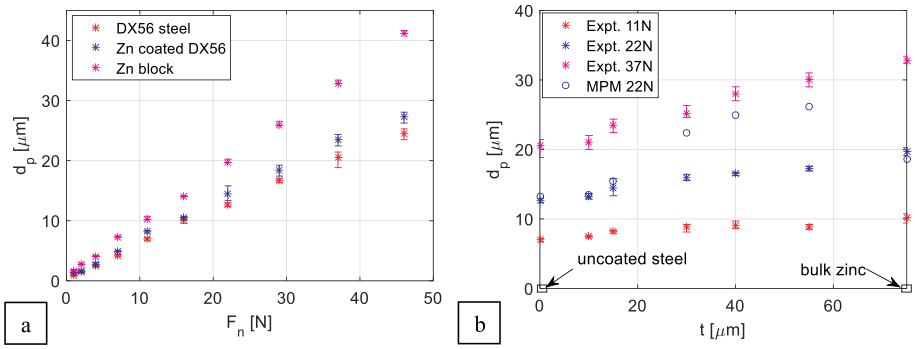


**Fig. 18.** (a) Comparison of ploughing depths obtained from ploughing experiments by 1 mm indenter with Quaker lubricated DX56 steel sheet, 15 μm thick zinc coated steel sheet, and pure zinc block. (b) Effect of coating thickness on ploughing depth for applied loads of 11, 22 and 37 N obtained from ploughing experiments and compared with MPM simulations for 22 N load with 1 mm diameter ball. (MPM model parameters: Tables 3–5).

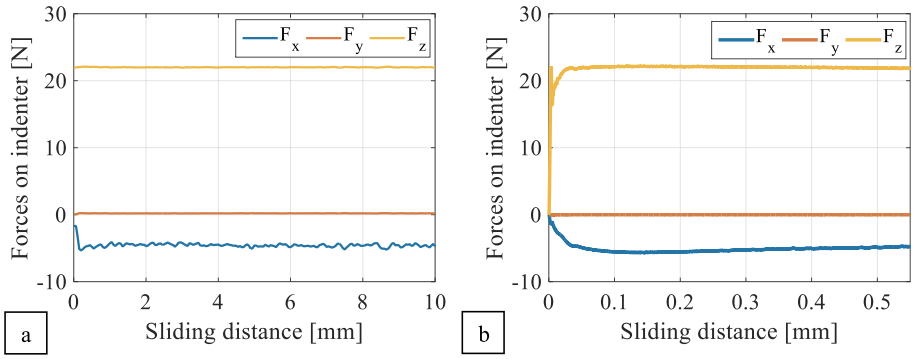


**Fig. 19.** Forces acting on a 1 mm diameter spherical indenter ploughing in $x$ direction on a lubricated, 15 μm thick, zinc coated steel sheet at 22 N normal load in (a) experiments and (b) MPM simulations.

0.0015, $z_1 = 0.997$ and $c_1 = 0.0046$, $z_1 = 0.999$ are obtained for 1 mm and 3 mm dia. balls respectively. Also, from equation (8.2), $\tau_{bl} = C_p \bar{P}^{n_p}$ where, $C_p = 0.32$, $n_p = 0.95$ and $\bar{P} = F_n/A_{xy}$ (see Table 5). By substituting the power law relations, $\mu_{sh}$ is given as a function of applied load $F_n$ in equation (9.2). The total coefficient of friction $\mu$ is taken as the sum of $\mu_{sh}$ and $\mu_{pl}$.

$$\mu_{pl} = H_c \frac{A_{yz}}{F_n} = \frac{H_c}{F_n} b_1 d_p^{y_1} = \frac{H_c}{F_n} b_1 \left(a_1 F_n^{x_1}\right)^{y_1} \tag{9.1}$$

$$\mu_{sh} = \tau_{sh} \frac{A_{xy}}{F_n} = C_p \left(\frac{F_n}{A_{xy}}\right)^{n_p} \left(\frac{A_{xy}}{F_n}\right) = C_p \left(\frac{c_1 d_p^{z_1}}{F_n}\right)^{1-n_p} = C_p \left(c_1 \left(a_1 F_n^{x_1}\right)^{z_1 - 1}\right)^{1-n_p} \tag{9.2}$$

The analytical coefficient of friction relations obtained by curve fitting are plotted in Fig. 22. A good agreement is shown for the 3 mm diameter indenter in Fig. 22b. The increase in $\mu_{pl}$ for the 3 mm ball is smaller than the 1 mm ball as expected from the lower plastic deformation with the larger indenter. The analytical under predicts the coefficient of friction for 1 mm ball in Fig. 22a. Although a constant hardness is assumed, the increase in hardness due to strain hardening is ignored in the simple analysis shown in Fig. 22. In reality, the increase in hardness is higher for 1 mm ball where higher ploughing depths result in higher hardening and higher hardness. From the results in Fig. 22a, the analytical model can be used to predict ploughing friction given the experimental data on the ploughing depths in a substrate.

The presence of zinc coating on the steel substrate results in a reduced coefficient of friction in ploughing as compared to both the zinc block and the steel substrate (see Fig. 23a). This is because the presence

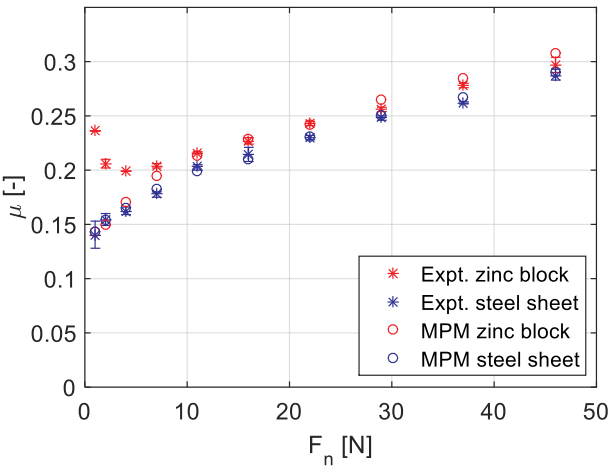


**Fig. 20.** Comparison of the coefficient of friction obtained from MPM model and ploughing experiments on Quaker lubricated zinc block and DX56 steel sheet by 1 mm diameter ball [47]. (MPM model parameters: Tables 3–5).

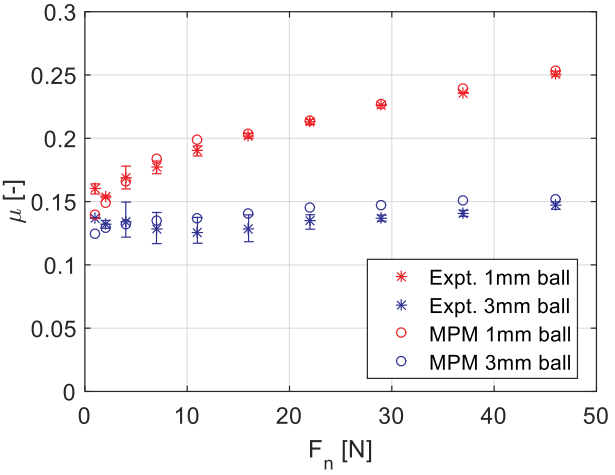


**Fig. 21.** Coefficient of friction for load controlled tests carried out with indenters of diameter 1 mm and 3 mm on lubricated zinc coated steel sheet (zinc coating thickness of 15 μm) with the linear sliding friction tester and MPM-ploughing model that includes the material model parameters from Tables 3 and 4 and interfacial friction model parameters in Table 5. (MPM model parameters: Tables 3–5).

of hard steel substrate underneath the zinc reduces the ploughing depth in the zinc (see Fig. 17) and hence $\mu_{pl}$. Furthermore, the interfacial shear strength of Quaker lubricant on zinc coating is lower as compared to that on DX56 steel substrate as shown in Fig. 10b. As interfacial shear has a major contribution to the overall coefficient of friction for large indenters [48], the lower boundary layer shear strength of the zinc coating combined with its low plastic deformation during ploughing contribute to a lower coefficient of friction in the zinc coating compared to bulk zinc and steel. At low normal loads, both the bulk zinc and the zinc coating have higher coefficient of friction. This could be due to asperity interlocking and high interfacial shear strength (see Fig. 4a) for the rough zinc surface.

The effect of coating thickness on the overall coefficient of friction for the soft zinc coating on the steel substrate is shown in Fig. 23b. The coefficient of friction was measured from ploughing experiments on zinc coatings with coating thickness of 10, 15, 30, 40 and 55 μm for 11, 22 and 37 N loads and MPM simulations for the same coating thickness at 22 N load. The coefficient of friction decreases with increase in coating thickness up to 15 μm and then increases with the coating thickness until the bulk zinc (infinite coating thickness). The change in coefficient of friction with zinc coating thickness resembles the theoretical relation between the coefficient of friction and the coating thickness for soft coatings shown in Fig. 4a. A higher coefficient of friction for thicker unpolished coatings, obtained with the MPM simulations could be explained due to the corresponding increase in simulated ploughing depths, as shown in Fig. 18b.

## 5. Conclusion

The coating thickness, substrate material properties and applied load have been varied to study their effect on the ploughing friction and ploughing depth. An analytical model is developed to predict the coefficient of friction and wear track depth of a single asperity ploughing through a coated or uncoated substrate and also validated using the using the MPM based-ploughing model. The ploughing behaviour of a zinc coating on a steel substrate has been numerically modelled and validated to good agreement using the MPM-based ploughing model and ploughing experiments. The analytical model is calibrated relative to the experimental data and then used to explain the variation in coefficient of friction with applied load and indenter size in ploughing experiments. The analytical model is also able to predict the effect of the coating thickness and substrate hardness on the coefficient of friction and ploughing depth for various normal loads in the ploughing experiments. Therefore, it can be concluded that friction in ploughing of a coated system is a function of the material properties (flow/yield curve) of the coating and the substrate, the shear strength of the contacting interfaces and the coating thickness.

## Declaration of competing interest

None.

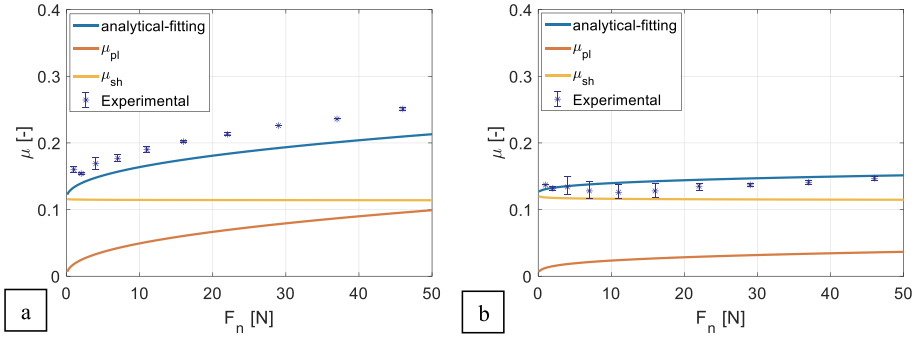


**Fig. 22.** Effect of asperity shape on ploughing coefficient of friction studied using analytical model and curve fitting for (a) 1 mm diameter indenter (b) 3 mm diameter indenter sliding on zinc coated steel.

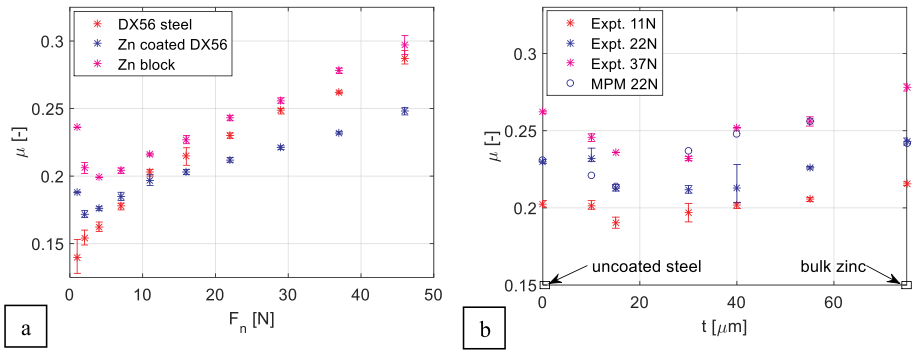


**Fig. 23.** (a) Comparison of coefficient of friction obtained from ploughing experiments by 1 mm indenter with Quaker lubricated DX56 steel sheet, 15 μm thick zinc coated steel sheet, and pure zinc block. (b) Effect of coating thickness $t$ on coefficient of friction at loads of 11, 22 and 37 N obtained from ploughing experiments and compared with MPM model for 22 N load with 1 mm diameter ball. (MPM model parameters: Tables 3–5).

## CRediT authorship contribution statement

**Tanmaya Mishra:** Methodology, Investigation, Data curation, Visualization, Validation, Software, Writing - original draft. **Matthijn de Rooij:** Funding acquisition, Project administration, Supervision, Conceptualization, Methodology, Writing - review & editing. **Meghshyam Shisode:** Resources, Software, Writing - review & editing. **Javad Hazrati:** Resources, Formal analysis, Writing - review & editing. **Dirk J. Schipper:** Project administration, Funding acquisition, Supervision, Writing - review & editing.

## Acknowledgments

This research was carried out under project number S22.1.14520a in the framework of the Partnership Program of the Materials innovation institute M2i (www.m2i.nl) and the Technology Foundation TTW (www.stw.nl), which is part of the Netherlands Organization for Scientific Research (www.nwo.nl). The authors would like to greatly acknowledge Dr.ir. Jeroen van Beeck from Tata Steel Europe R&D for their technical guidance and provision of Bergström-van Liempt material model parameters for DX56 steel and the stress-strain curves for the zinc block.

## Appendix A. Supplementary data

Supplementary data to this article can be found online at https://doi.org/10.1016/j.wear.2020.203219.

## References

[1] R. ter Haar, Friction in Sheet Metal Forming, the Influence of (Local) Contact Conditions and Deformation, PhD thesis, University of Twente, The Netherlands, 1996, ISBN 90-9009296-X, 1996.
[2] H.C. Shih, Friction of Coated Automotive Steels in Stamping. Encyclopedia of Tribology, Springer, Boston, MA, 2013, https://doi.org/10.1007/978-0-387-92897-5_623, 1359-1365.
[3] Y. Kim, H. Kim, Y.T. Keum, Evaluation of frictional characteristic for Zinc-coated steel sheet, Met. Mater. 6 (4) (2000) 323–329, https://doi.org/10.1007/BF0302807.
[4] Y. Zhang, Q.P. Cui, F.Q. Shao, J.S. Wang, H.Y. Zhao, Influence of air-knife wiping on coating thickness in hot-dip galvanizing, J. Iron Steel Res. Int. 19 (6) (2012) 70–78, https://doi.org/10.1016/S1006-706X(12)60130-7.
[5] S. Lee, M. Joun, D. Kim, J. Lee, Effect of elastic-plastic behavior of coating layer on drawability and frictional characteristic of galvannealed steel sheets, J. Mech. Sci. Technol. 30 (7) (2016) 3313–3319, https://doi.org/10.1007/s12206-016-0640-5.
[6] A.J.D. Westeneng, Modelling of Contact and Friction in Deep Drawing Processes, PhD thesis, University of Twente, The Netherlands, 2003, ISBN 90-365-1549-1, 2001.
[7] F.P. Bowden, A.J.W. Moore, D. Tabor, The ploughing and adhesion of sliding metals, J. Appl. Phys. 14 (2) (1943) 80–91, https://doi.org/10.1063/1.1714954.
[8] K. Holmberg, H. Ronkainen, A. Matthews, Tribology of thin coatings, Ceram. Int. 26 (7) (2000) 787–795, https://doi.org/10.1016/S0272-8842(00)00015-8.
[9] S.J. Bull, E.G. Berasetegui, An overview of the potential of quantitative coating adhesion measurement by scratch testing, Tribol. Int. 39 (2) (2006) 99–114, https://doi.org/10.1016/j.triboint.2005.04.013.
[10] M.B. de Rooij, Tribological Aspects of Unlubricated Deep-Drawing Process, PhD thesis, University of Twente, The Netherlands, 1998, ISBN 90-3651218-2.
[11] N. Panich, Y. Sun, Effect of penetration depth on indentation response of soft coatings on hard substrates: a finite element analysis, Surf. Coating. Technol. 182 (2-3) (2004) 342–350, https://doi.org/10.1016/j.surfcoat.2003.07.002.
[12] C. Gamonpilas, E.P. Busso, On the effect of substrate properties on the indentation behaviour of coated systems, Mater. Sci. Eng., A 380 (1-2) (2004) 52–61, https://doi.org/10.1016/j.msea.2004.04.038.
[13] Z.H. Xu, D. Rowcliffe, Finite element analysis of substrate effects on indentation behaviour of thin films, Thin Solid Films 447 (2004) 399–405, https://doi.org/10.1016/S0040-6090(03)01071-X.
[14] Z. Liu, A. Neville, R.L. Reuben, The effect of film thickness on initial friction of elastic-plastically rough surface with a soft thin metallic film, J. Tribol. 124 (3) (2002) 627–636, https://doi.org/10.1115/1.1454103.
[15] J. Lackner, L. Major, M. Kot, Microscale interpretation of tribological phenomena in Ti/TiN soft-hard multilayer coatings on soft austenite steel substrates, Bull. Pol. Acad. Sci. Tech. Sci. 59 (3) (2011) 343–355, https://doi.org/10.2478/v10175-011-0042-x.
[16] J. Cao, Z. Yin, H. Li, G. Gao, Tribological studies of soft and hard alternated composite coatings with different layer thicknesses, Tribol. Int. 110 (2017) 326–332, https://doi.org/10.1016/j.triboint.2017.02.039.
[17] J.D. Kamminga, G.C.A.M. Janssen, Experimental discrimination of plowing friction and shear friction, Tribol. Lett. 25 (2) (2007) 149–152, https://doi.org/10.1007/s11249-006-9135-3.
[18] M.A. Sherbiney, J. Halling, Friction and wear of ion-plated soft metallic films, Wear 45 (2) (1977) 211–220, https://doi.org/10.1016/0043-1648(77)90075-8.
[19] J. Halling, Surface coatings materials conservation and optimum tribological performance, Tribol. Int. 12 (5) (1979) 203–208, https://doi.org/10.1016/0301-679X(79)90189-0.
[20] J. Halling, The tribology of surface films, Thin Solid Films 108 (2) (1983) 103–115, https://doi.org/10.1016/0040-6090(83)90496-0.
[21] W.R. Chang, An elastic-plastic contact model for a rough surface with an ion-plated soft metallic coating, Wear 212 (2) (1997) 229–237, https://doi.org/10.1016/S0043-1648(97)00148-8.
[22] H. Jiang, R. Browning, J.D. Whitcomb, M. Ito, M. Shimouse, T.A. Chang, H.J. Sue, Mechanical modeling of scratch behavior of polymeric coatings on hard and soft substrates, Tribol. Lett. 37 (2) (2010) 159–167, https://doi.org/10.1007/s11249-009-9505-8.
[23] M.M. Hossain, S. Xiao, H.J. Sue, M. Kotaki, Scratch behavior of multilayer polymeric coating systems, Mater. Des. 128 (2017) 143–149, https://doi.org/10.1016/j.matdes.2017.05.012.
[24] K. Holmberg, A. Laukkanen, H. Ronkainen, K. Wallin, S. Varjus, J. Koskinen, Tribological contact analysis of a rigid ball sliding on a hard coated surface: Part I: modelling stresses and strains, Surf. Coating. Technol. 200 (12-13) (2006) 3793–3809, https://doi.org/10.1016/j.surfcoat.2005.03.040.
[25] D. Meng, Y.G. Li, Z.T. Jiang, M.K. Lei, Scratch behavior and FEM modelling of Cu/Si (100) thin films deposited by modulated pulsed power magnetron sputtering, Surf. Coating. Technol. 363 (2019) 25–33, https://doi.org/10.1016/j.surfcoat.2019.02.008.
[26] G. Kermouche, N. Aleksy, J.L. Loubet, J.M. Bergheau, Finite element modeling of the scratch response of a coated time-dependent solid, Wear 267 (11) (2009) 1945–1953, https://doi.org/10.1016/j.wear.2009.05.005.
[27] T.H. Fang, C.H. Liu, S.T. Shen, S.D. Prior, L.W. Ji, J.H. Wu, Nanoscratch behavior of multi-layered films using molecular dynamics, Appl. Phys. A 90 (4) (2008) 753–758, https://doi.org/10.1007/s00339-007-4351-8.
[28] T.H. Fang, J.H. Wu, Molecular dynamics simulations on nanoindentation mechanisms of multilayered films, Comput. Mater. Sci. 43 (4) (2008) 785–790, https://doi.org/10.1016/j.commatsci.2008.01.066.
[29] A.V. Bolesta, V.M. Fomin, Molecular dynamics simulation of sphere indentation in a thin copper film, Phys. Mesomech. 12 (3-4) (2009) 117–123, https://doi.org/10.1016/j.physme.2009.07.003.

[30] T. Akabane, Y. Sasajima, J. Onuki, Coating adhesion evaluation by nanoscratching simulation using the molecular dynamics method, Jpn. J. Appl. Phys. 46 (5R) (2007) 3024, https://doi.org/10.1143/JJAP.46.3024.
[31] J. Malzbender, G. de With, J.M.J. Den Toonder, Determination of the elastic modulus and hardness of sol–gel coatings on glass: influence of indenter geometry, Thin Solid Films 372 (1-2) (2000) 134–143, https://doi.org/10.1016/S0040-6090(00)01025-7.
[32] R. Saha, W.D. Nix, Effects of the substrate on the determination of thin film mechanical properties by nanoindentation, Acta Mater. 50 (1) (2002) 23–38, https://doi.org/10.1016/S1359-6454(01)00328-7.
[33] R. Saha, Z. Xue, Y. Huang, W.D. Nix, Indentation of a soft metal film on a hard substrate: strain gradient hardening effects, J. Mech. Phys. Solid. 49 (9) (2001) 1997–2014, https://doi.org/10.1016/S0022-5096(01)00035-7.
[34] J.M. Challen, P.L.B. Oxley, An explanation of the different regimes of friction and wear using asperity deformation models, Wear 53 (2) (1979) 229–243, https://doi.org/10.1016/0043-1648(79)90080-2.
[35] Z.S. Ma, Y.C. Zhou, S.G. Long, C. Lu, On the intrinsic hardness of a metallic film/substrate system: indentation size and substrate effects, Int. J. Plast. 34 (2012) 1–11, https://doi.org/10.1016/j.ijplas.2012.01.001.
[36] H. Gao, C.H. Chiu, J. Lee, Elastic contact versus indentation modeling of multi-layered materials, Int. J. Solid Struct. (1992), https://doi.org/10.1016/0020-7683(92)90004-D.
[37] M.V. Swain, J. Menčík, Mechanical property characterization of thin films using spherical tipped indenters, Thin Solid Films 253 (1–2) (1994) 204–211, https://doi.org/10.1016/0040-6090(94)90321-2.
[38] R.S. Timsit, C.V. Pelow, Shear strength and tribological properties of stearic acid films—Part I: on glass and aluminum-coated glass, J. Tribol. 114 (1) (1992) 150–158, https://doi.org/10.1115/1.2920854.
[39] R.S. Timsit, C.V. Pelow, Shear strength and tribological properties of stearic acid films—Part II: on gold-coated glass, J. Tribol. 114 (1) (1992) 159–166, https://doi.org/10.1115/1.2920855.
[40] B.J. Briscoe, D.C.B. Evans, The shear properties of Langmuir—blodgett layers, Proc. Roy. Soc. Lond. Math. Phys. Sci. 380 (1779) (1982) 389–407, https://doi.org/10.1098/rspa.1982.0048.
[41] N. Coni, M.L. Gipiela, A.S.C.M. D'Oliveira, P.V.P. Marcondes, Study of the mechanical properties of the hot dip galvanized steel and galvalume®, J. Braz. Soc. Mech. Sci. Eng. 31 (4) (2009) 319–326, https://doi.org/10.1590/S1678-58782009000400006.
[42] R. Parisot, S. Forest, A.F. Gourgues, A. Pineau, D. Mareuse, Modeling the mechanical behavior of a multicrystalline zinc coating on a hot-dip galvanized steel sheet, Comput. Mater. Sci. 19 (1–4) (2000) 189–204, https://doi.org/10.1016/S0927-0256(00)00155-5.
[43] G.M. Song, W.G. Sloof, Y.T. Pei, J.T.M. De Hosson, Interface fracture behavior of zinc coatings on steel: experiments and finite element calculations, Surf. Coating. Technol. 201 (7) (2006) 4311–4316, https://doi.org/10.1016/j.surfcoat.2006.08.046.
[44] G.M. Song, J.T.M. De Hosson, W.G. Sloof, Y.T. Pei, Evaluation of interface adhesion of hot-dipped zinc coating on TRIP steel with tensile testing and finite element calculation, WIT Trans. Eng. Sci. 91 (2015) 3–14, https://doi.org/10.2495/SECM150011.
[45] Y.T. Pei, G.M. Song, W.G. Sloof, J.T.M. De Hosson, A methodology to determine anisotropy effects in non-cubic coatings, Surf. Coating. Technol. 201 (16-17) (2007) 6911–6916, https://doi.org/10.1016/j.surfcoat.2006.11.044.
[46] R.R. Tohid, S.J. Bull, Getting accurate nanoindentation data from time-dependent and microstructural effects of zinc, Int. J. Mater. Res. 98 (5) (2007) 353–359, https://doi.org/10.3139/146.101477.
[47] T. Mishra, G.C. Ganzenmüller, M. de Rooij, M. Shisode, J. Hazrati, D.J. Schipper, Modelling of ploughing in a single-asperity sliding contact using material point method, Wear 418 (2019) 180–190, https://doi.org/10.1016/j.wear.2018.11.020.
[48] T. Mishra, M. de Rooij, M. Shisode, J. Hazrati, D.J. Schipper, Characterization of interfacial shear strength and its effect on ploughing behaviour in single-asperity sliding, Wear 436-437 (2019), https://doi.org/10.1016/j.wear.2019.203042, 203042.
[49] J. Halling, M.A. Sherbiney, The role of surface topography in the friction of soft metallic films, in: Tribology 1978: Materials Performance and Conservation IMechE. Tribology Convention, Swansea, 1978. ISBN: 0852984006.
[50] J. Halling, R.D. Arnell, Ceramic coatings in the war on wear, Wear 100 (1–3) (1984) 367–380, https://doi.org/10.1016/0043-1648(84)90022-X.
[51] D. Tabor, The Hardness of Metals, Oxford university press, London, 2000, ISBN 9780198507765.
[52] T. Mishra, M. de Rooij, M. Shisode, J. Hazrati, D.J. Schipper, A material point method based ploughing model to study the effect of asperity geometry on the ploughing behaviour of an elliptical asperity, Tribol. Int. 140 (2020) 106017, https://doi.org/10.1016/j.triboint.2019.106017.
[53] J. Strutzenberger, J. Faderl, Solidification and spangle formation of hot-dip-galvanized zinc coatings, Metall. Mater. Trans. 29 (2) (1998) 631–646, https://doi.org/10.1007/s11661-998-0144-8.
[54] P.E. Senseny, J. Duffy, R.H. Hawley, Experiments on strain rate history and temperature effects during the plastic deformation of close-packed metals, J. Appl. Mech. 45 (1) (1978) 60–66, https://doi.org/10.1115/1.3424274.
[55] P. Van Liempt, Workhardening and substructural geometry of metals, J. Mater. Process. Technol. 45 (1–4) (1994) 459–464, https://doi.org/10.1016/0924-0136(94)90382-4.
[56] H. Vegter, On the Plastic Behaviour of Steel during Sheet Forming, PhD thesis, University of Twente, The Netherlands, 1993, ISBN 9789090043739.
[57] G.R. Johnson, W.H. Cook, Fracture characteristics of three metals subjected to various strains, strain rates, temperatures and pressures, Eng. Fract. Mech. 21 (1) (1985) 31–48, https://doi.org/10.1016/0013-7944(85)90052-9.
[58] H. Swift, Plastic instability under plane stress, J. Mech. Phys. Solid. 1 (1) (1952) 1–18, https://doi.org/10.1016/0022-5096(52)90002-1.
[59] S. Bardenhagen, E. Kober, The Generalized interpolation material point method, Comput. Model. Eng. Sci. 5 (6) (2004) 477–495, https://doi.org/10.3970/cmes.2004.005.477.